

## **Reply to comments raised by Referee #1.**

The original comments are in plain texts, and our replies are in **bold texts**.

This study investigates the C<sub>3</sub>H<sub>8</sub> retrieval from ground-based FTIR spectra at Xianghe, and discuss the C<sub>3</sub>H<sub>8</sub> column variation in North China, based on these new FTIR measurements. The technical details and uncertainty discussion are generally well provided in current form, but the result part, such as data comparison and trend explanation, are somewhat less satisfactory. Overall, I suggest the publication on AMT after presenting more information for data interpretation. Specific suggestions are listed below.

### **First of all, we would like to thank you for the comments and suggestions.**

1. Method 2.3: Line 20-25: It is still not clear why perform a profile retrieval for H<sub>2</sub>O column concentration. Because each species could have large variability in vertical scale. Moreover, suggest providing more technical details about the how to perform a profile retrieval.

### **More information are added now.**

**Original text:** “To reduce the impact of uncertainties about the abundances of these species, these column abundances are retrieved along with the target gas mole fractions; only for H<sub>2</sub>O we perform a profile retrieval, because of its large variability.”

**Revised text:** “To reduce the impact of uncertainties about the abundances of these species, CH<sub>4</sub>, O<sub>3</sub> and HDO columns are retrieved along with the target gas mole fractions. For these three species, their profile shapes are fixed and only scaling factors are retrieved simultaneously. As H<sub>2</sub>O absorption lines are relatively strong (Table 1) and H<sub>2</sub>O variability is large in the atmosphere, we perform a profile retrieval for H<sub>2</sub>O. Therefore, the state vector includes CH<sub>4</sub>, O<sub>3</sub> and HDO columns, as well as 47-layers' C<sub>3</sub>H<sub>8</sub> and H<sub>2</sub>O mole fractions.”

2. Section 3.2: Since the large difference exists for seasonal variation of C<sub>3</sub>H<sub>8</sub> column concentration between model and FTIR measurements, it would be better not present this comparison in the main text, unless the authors could provide more evidence or information to explain these differences. For example, the authors could collect some surface observation of C<sub>3</sub>H<sub>8</sub> concentration in Xianghe or surrounding regions that used for comparison to FTIR retrieval near the surface.

**Thanks for the suggestion. Unfortunately, there is no surface observation of C<sub>3</sub>H<sub>8</sub> in Xianghe or surrounding regions. Currently we do not have solid conclusion to fully understand the discrepancy between the FTIR measurements and the model simulations. In the revised version, this part has been removed.**

3. Section 3.3 Line 20-25: What is the significance by providing the ratio of  $\Delta\text{C}_2\text{H}_6$  to  $\Delta\text{C}_3\text{H}_8$ ? What does the trend of this ratio mean?

Since  $\text{C}_2\text{H}_6$  and  $\text{C}_3\text{H}_8$  are co-emitted by oil gas sources (Li et al., 2017; Bourtsoukidis et al., 2019) and  $\text{C}_2\text{H}_6$  and  $\text{C}_3\text{H}_8$  have similar lifetimes with about 2-8 weeks, the ratio of  $\Delta\text{C}_2\text{H}_6$  to  $\Delta\text{C}_3\text{H}_8$  can represent the emission ratios of  $\text{C}_2\text{H}_6$  to  $\text{C}_3\text{H}_8$  in this region.

The trend of this ratio represents the trend of the emission ratio in this region. As our FTIR measurements do not show a clear trend in  $\Delta\text{C}_2\text{H}_6/\Delta\text{C}_3\text{H}_8$ , it is inferred that the emission ratios of  $\text{C}_2\text{H}_6$  to  $\text{C}_3\text{H}_8$  in this region remain unchanged between 2018 and 2022.

4. Section 3.4: The authors compare FTIR measurement to MkIV data here, but the basic information about MkIV measurement were not well described. Readers might be very interested about the principle of technique used for  $\text{C}_3\text{H}_8$  measurement in MkIV and the accuracy of these data. Based on these information, we can rule out the systematic difference deviation between FTIR and MkIV.

Thanks for the suggestion. More information about the MKIV  $\text{C}_3\text{H}_8$  data are added in the revised version.

“MKIV  $\text{C}_3\text{H}_8$  data uses the GFIT inverse retrieval code to derive the  $\text{C}_3\text{H}_8$  columns from the MKIV observed spectra between 2964.5 and 2970  $\text{cm}^{-1}$  with a spectral resolution of 0.5  $\text{cm}^{-1}$ . The mean uncertainties of the MKIV retrieved  $\text{C}_3\text{H}_8$  and  $\text{C}_2\text{H}_6$  column are estimated to be around  $8 \times 10^{15}$  molecules/ $\text{cm}^2$  and  $7 \times 10^{14}$  molecules/ $\text{cm}^2$ , respectively, which are also provided by Toon et al., (2021).”

#### References:

Bourtsoukidis, E., Ernle, L., Crowley, J. N., Lelieveld, J., Paris, J.-D., Pozzer, A., Walter, D., and Williams, J.: Non-methane hydrocarbon ( $\text{C}_2\text{-C}_8$ ) sources and sinks around the Arabian Peninsula, *Atmos. Chem. Phys.*, 19, 7209–7232, <https://doi.org/10.5194/acp-19-7209-2019>, 2019.

Li, M., Liu, H., Geng, G., Hong, C., Liu, F., Song, Y., Tong, D., Zheng, B., Cui, H., Man, H., Zhang, Q., and He, K.: Anthropogenic emission inventories in China: a review, *Natl. Sci. Rev.*, 4, 834–866, <https://doi.org/10.1093/nsr/nwx150>, 2017.

Toon, G. C., Blavier, J.-F. L., Sung, K., and Yu, K.: Spectrometric measurements of atmospheric propane ( $\text{C}_3\text{H}_8$ ), *Atmos. Chem. Phys.*, 21, 10727–10743, <https://doi.org/10.5194/acp-21-10727-2021>, 2021.

## Reply to comments raised by Referee #2.

The original comments are in plain texts, and our replies are in **bold texts**.

General comments:

This study used ground-based FTIR Mid-infrared observations at Xianghe to retrieve C<sub>3</sub>H<sub>8</sub> column through optimal estimation approach. Compared with CH<sub>4</sub> and H<sub>2</sub>O, the absorption of C<sub>3</sub>H<sub>8</sub> is weak at 2964.5-2970.0 cm<sup>-1</sup>, thus retrieving C<sub>3</sub>H<sub>8</sub> is challenging. Although the authors conducted uncertainty analysis, I still have some concerns about the accuracy and importance of the C<sub>3</sub>H<sub>8</sub> retrievals.

**First of all, we would like to thank you for the comments and suggestions.**

Specific comments:

1. Due to the weak absorption of C<sub>3</sub>H<sub>8</sub>, I suspect that the a posteriori C<sub>3</sub>H<sub>8</sub> strongly depends on a priori C<sub>3</sub>H<sub>8</sub>. Figure 6 shows the seasonal variation of FTIR C<sub>3</sub>H<sub>8</sub> is different from the two model simulations. How is the monthly variation of the a priori C<sub>3</sub>H<sub>8</sub>? Is it similar to the FTIR retrieval? It would be interesting to see to how the a posteriori C<sub>3</sub>H<sub>8</sub> vary if different a priori profile (for example, using profiles from CAMS and WACCM as a priori) is used.

**Thanks for the suggestion and comment. In this study, the a priori profile of C<sub>3</sub>H<sub>8</sub> is derived from the mean of WACCM model simulations between 1980 and 2040. The a priori mole fraction profile is fixed, which does not vary with time. By using a fixed a priori profile, the retrieved C<sub>3</sub>H<sub>8</sub> mole fraction is less affected by the a priori variation. More information is added in the revised version. In addition, we added the a priori C<sub>3</sub>H<sub>8</sub> columns in the left panel of Figure 5. Note that the a priori mole fraction is fixed, while the a priori columns vary with surface pressure, with a maximum in winter and minimum in summer.**

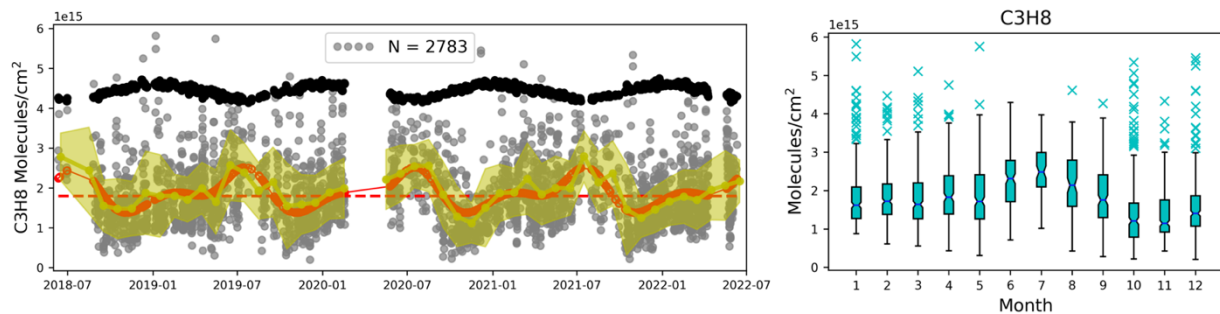


Figure 5. Left panel shows the time series of FTIR a priori columns (black dots), individual C3H8 column measurements (grey dots), monthly means (yellow line), monthly stds (yellow shade), and periodic function fitting (red solid line) and the fitted offset (red dashed line). Right panel: the monthly box plot of the FTIR retrieved C3H8 columns. The bottom and top bars represent the 10% and 90% percentiles of the datasets and the blue crosses are the extremely high values above 90%.

2. As CH4 and H2O have stronger absorption than C3H8, and CH4 and H2O absorption lines are not perfectly fitted, how it will affect the accuracy of C3H8 retrieval should be discussed.

Thanks for the comment. More discussion about CH4 and H2O impacts are added in the revised version. Particularly, the retrieval error of the C3H8 column from the CH4 and H2O spectroscopy uncertainty are re-calculated and added in Table 3.

3. In Sect. 2.4, how uncertainty is calculated? Apparently, we cannot get  $x_i$  and  $b_i$ . More details are needed.

Thanks for the comment. More information about the uncertainties are added in the revised version.

It is assumed that 10% of the a priori profile is used to derive the diagonal values of the systematic covariance matrix  $S_a^{sys} = \sigma_i^2$ , and the off-diagonal values of  $S_a^{sys}$  are calculated as  $S_a^{sys} = \sigma_i \sigma_j$  (von Clarmann 2014 AMT). The covariance matrix derived from the WACCM 61-years' monthly means are set to the random covariance matrix  $S_a^{ran}$ .

Regarding the model parameter uncertainties in the Table 3, the systematic/random  $S_b$  matrix was created by the mean/standard deviation of the differences between NCEP and ERA5 at Xianghe. The random deviation is about 2K, and the systematic deviation is about 1.5K for the whole vertical range. For the target spectroscopic parameters, the relative uncertainties of C3H8 is set to 4% according to the PLL database. For the CH4 and H2O spectroscopy parameters, the relative uncertainty of 5% is derived from the HITRAN 2020 dataset. For the uncertainties of curvature, zshift, and SZA, we use the values provided by the SFIT4 algorithm (<https://wiki.ucar.edu/display/sfit4/SFIT4+Version+1.0.xx+Release>), which is recommended by the NDACC-IRWG community.

Toon, G. C., Blavier, J.-F. L., Sung, K., and Yu, K.: Spectrometric measurements of atmospheric propane (C<sub>3</sub>H<sub>8</sub>), *Atmos. Chem. Phys.*, 21, 10727–10743, <https://doi.org/10.5194/acp-21-10727-2021>, 2021. should be cited. It used observation around 2967 cm<sup>-1</sup> to retrieve C<sub>3</sub>H<sub>8</sub>.

**References:**

von Clarmann, T.: *Smoothing error pitfalls*, *Atmos. Meas. Tech.*, 7, 3023-3034, doi:10.5194/amt-7-3023-2014, 2014.

### **Reply to comments raised by Referee #3.**

The original comments are in plain texts, and our replies are in **bold texts**.

Review of "Atmospheric propane (C<sub>3</sub>H<sub>8</sub>) column retrievals from ground-based FTIR observations at Xianghe, China" by Zhou et al., amt-2024-67

This manuscript presents a 4 year data record of C<sub>3</sub>H<sub>8</sub> (and C<sub>2</sub>H<sub>6</sub>) column amount measurements at the Xianghe TCCON site. Retrievals are carried out from high resolution spectra in the 2964.5-2970.0 cm<sup>-1</sup> range (C<sub>3</sub>H<sub>8</sub> Q-branch). Several spectroscopic line lists are compared in terms of spectral fit quality. The uncertainty of retrieved C<sub>3</sub>H<sub>8</sub> columns is estimated and the seasonal variation, as well as the correlation of C<sub>3</sub>H<sub>8</sub> with other hydrocarbons, is discussed. Results are compared to two different models and to FTIR measurements at other sites.

The subject of this paper has relevance within the scope of AMT. New data are presented and I find the overall quality of presentation clear and concise.

Yet, the paper currently leaves the reader with a number of open questions. Since Toon et al. (2021) have already presented first measurements of C<sub>3</sub>H<sub>8</sub> with a similar methodology, I find that more work is needed with respect to the interpretation of the results before publication, so that this paper adds value to the existing literature. The big question to me is: Do we trust these column retrievals and if so, why are C<sub>3</sub>H<sub>8</sub> columns so low in Xianghe?

**First of all, we would like to thank you for the comments and suggestions.**

General comments:

G1: I am concerned that the retrieved C<sub>3</sub>H<sub>8</sub> values from this study do not line up with similar measurements and models. I do find it surprising that C<sub>3</sub>H<sub>8</sub> columns 50 km downwind of Beijing should be one order of magnitude lower than C<sub>3</sub>H<sub>8</sub> columns in Pasadena (10<sup>15</sup> vs. 10<sup>16</sup> molec/cm<sup>2</sup>). You mention on page 2: "we expect that the C<sub>2</sub>H<sub>6</sub> and C<sub>3</sub>H<sub>8</sub> concentrations are relatively high in this region" - I agree and would like to ask you to please expand your study in a way that resolves this apparent conflict. Similarly, it appears that the present measurements are in broad agreement with CAMS/WACCM during wildfire season in northern summer, but not during the winter when gas is being consumed. What are the atmospheric situations when you do observe high wintertime C<sub>3</sub>H<sub>8</sub>? Can we understand these results in the context of the existing measurements and models?

Thanks for the comments. We expect that the C<sub>2</sub>H<sub>6</sub> and C<sub>3</sub>H<sub>8</sub> concentrations are relatively high in this region, which is consistent with the model simulations (both CAMS and WACCM models). For example, the C<sub>3</sub>H<sub>8</sub> mole fraction in the CAMS model (Figure 1A) shows that Beijing region is a hotspot around the world, which is larger than Pasadena. When comparing the Xianghe FTIR measurements with MKIV measurements at JPL, the C<sub>3</sub>H<sub>8</sub> columns are much smaller than that at JPL. Two aspects may cause this. First, the uncertainty of the emission inventories used in the model is very large. Pétron et al., (2014) pointed out that the uncertainty in the C<sub>3</sub>H<sub>8</sub> emission estimate is larger than 30%, which is the sum of the relative uncertainty in the total CH<sub>4</sub> emission estimate and the relative uncertainty in the CH<sub>4</sub>-to-C<sub>3</sub>H<sub>8</sub> slope. What's more, the uncertainty of the emission can be much larger in a small region as compared to a national level. Secondly, the retrieval uncertainty of the MKIV measurements is also very large. Toon et al., (2021) reported the uncertainty of MKIV C<sub>3</sub>H<sub>8</sub> measurement is about  $8.0 \times 10^{15}$  molecules/cm<sup>2</sup>. More information has been added in discussion of the revised version.

The discrepancy in the seasonal variation between the FTIR measurements at Xianghe and model simulations (CAMS and WACCM) is also found at JPL, where the model shows a maximum in winter and a minimum in summer but the MKIV measurements also show a maximum in summer and a minimum in winter. First, we checked the sources and sinks in the model and tried to understand why the model shows a maximum in winter and a minimum in summer. The emission dataset used in the CAMS model is shown in Figure A2. The seasonal variation of C<sub>3</sub>H<sub>8</sub> emission is relatively small, with an amplitude of less than 15%. In addition, we also checked the OH seasonal variation in the CAMS model (Figure A3). The model shows that OH is high in summer, which is about 2 times larger than that in winter. Therefore, combining the sources and sinks in the model, the C<sub>3</sub>H<sub>8</sub> concentration in the model is larger in winter as compared to that in summer. However, as we motioned above, the uncertainty of the C<sub>3</sub>H<sub>8</sub> emission is relatively large (>30%), and the uncertainty of the OH in the model is also quite large. All these uncertainties may lead to a different seasonal variation of C<sub>3</sub>H<sub>8</sub>. Secondly, we checked the FTIR C<sub>3</sub>H<sub>8</sub> fitting residual and temporal variation of the FTIR measurements to understand whether there is an artificial in its seasonal variation or not. Figure A4 shows that there is no clear difference in the fitting residual between summer and winter. We also took a month in summer and winter, separately (Figure A5), and checked the temporal variation of C<sub>3</sub>H<sub>8</sub> and C<sub>2</sub>H<sub>6</sub> simultaneously. In both months, the FTIR measurements show that C<sub>3</sub>H<sub>8</sub> columns have a high correlation with C<sub>2</sub>H<sub>6</sub> columns. The day-to-day temporal variation observed by FTIR C<sub>2</sub>H<sub>6</sub> measurements can also be well captured by FTIR

C3H8 measurements. Therefore, we believe the FTIR C3H8 measurements are reliable in both seasons.

In summary, the discrepancy in the seasonal variation between the FTIR measurements at Xianghe and model simulations is probably caused by the model uncertainty. However, we have no solid conclusion. Following the comment and suggestion proposed by Referee #1, we have removed the section about the comparison between the FTIR measurements and model simulations in the revised version for now.

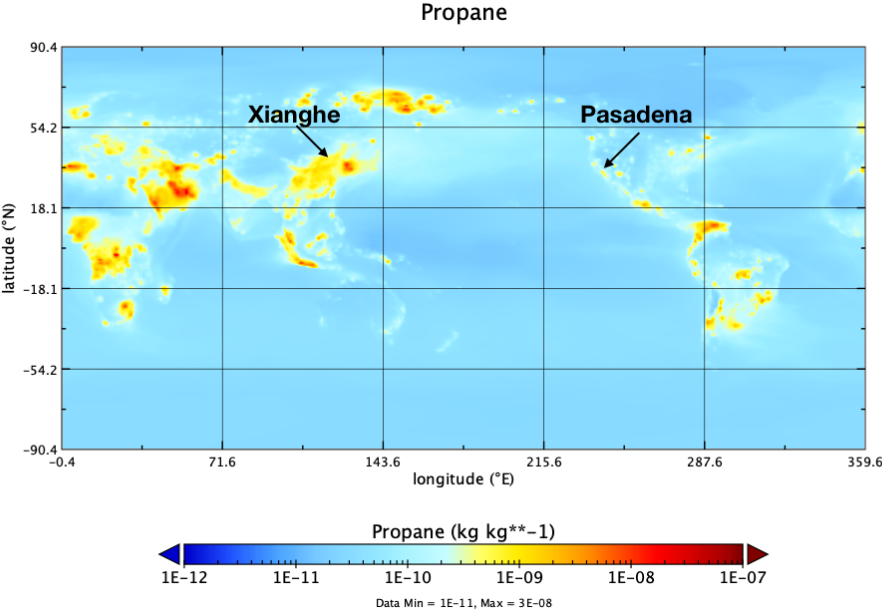


Figure A1. The C3H8 mass fraction near the surface in June 2020 from the CAMS model.



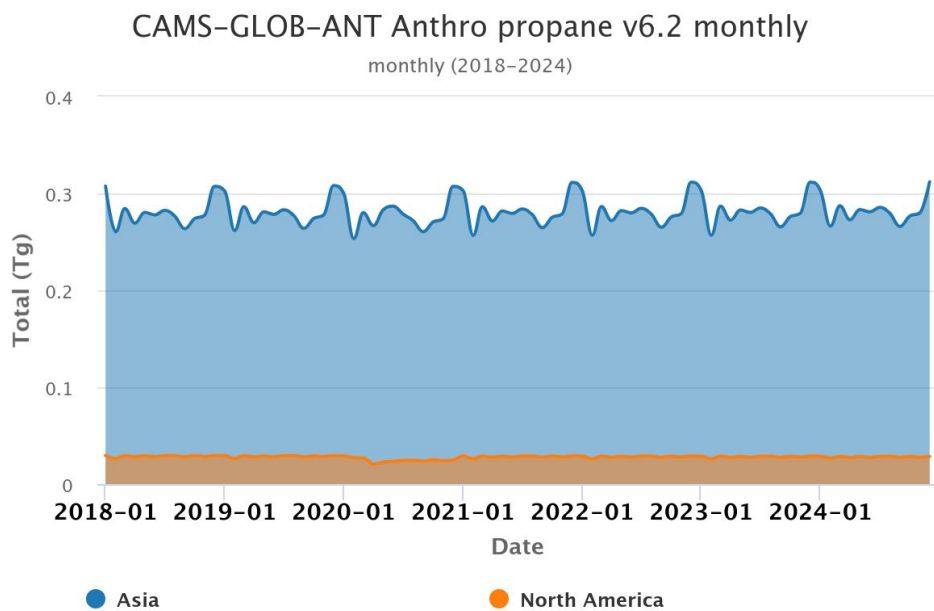


Figure A2. The time series of the C<sub>3</sub>H<sub>8</sub> monthly emissions in Asia and North America from the CAMS-GLOB-ANT database.

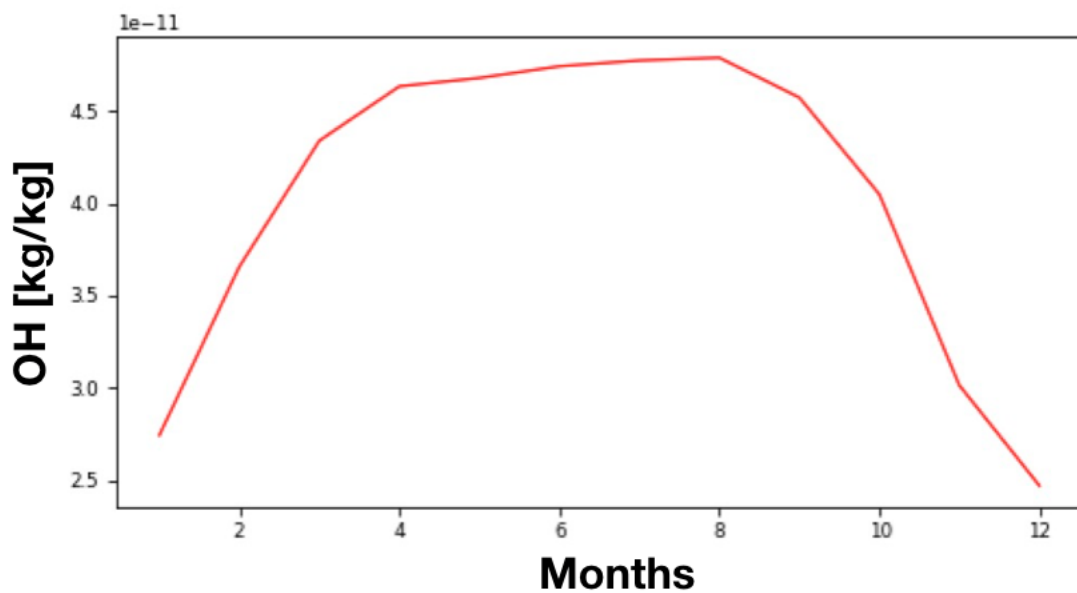


Figure A3. The seasonal variation of OH concentration near the surface at Xianghe from the CAMS model.

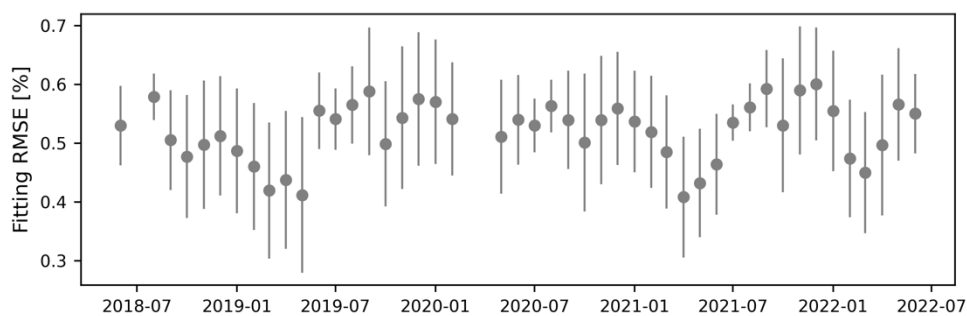


Figure A4. The time series of the monthly mean and SD of the fitting RMSEs.

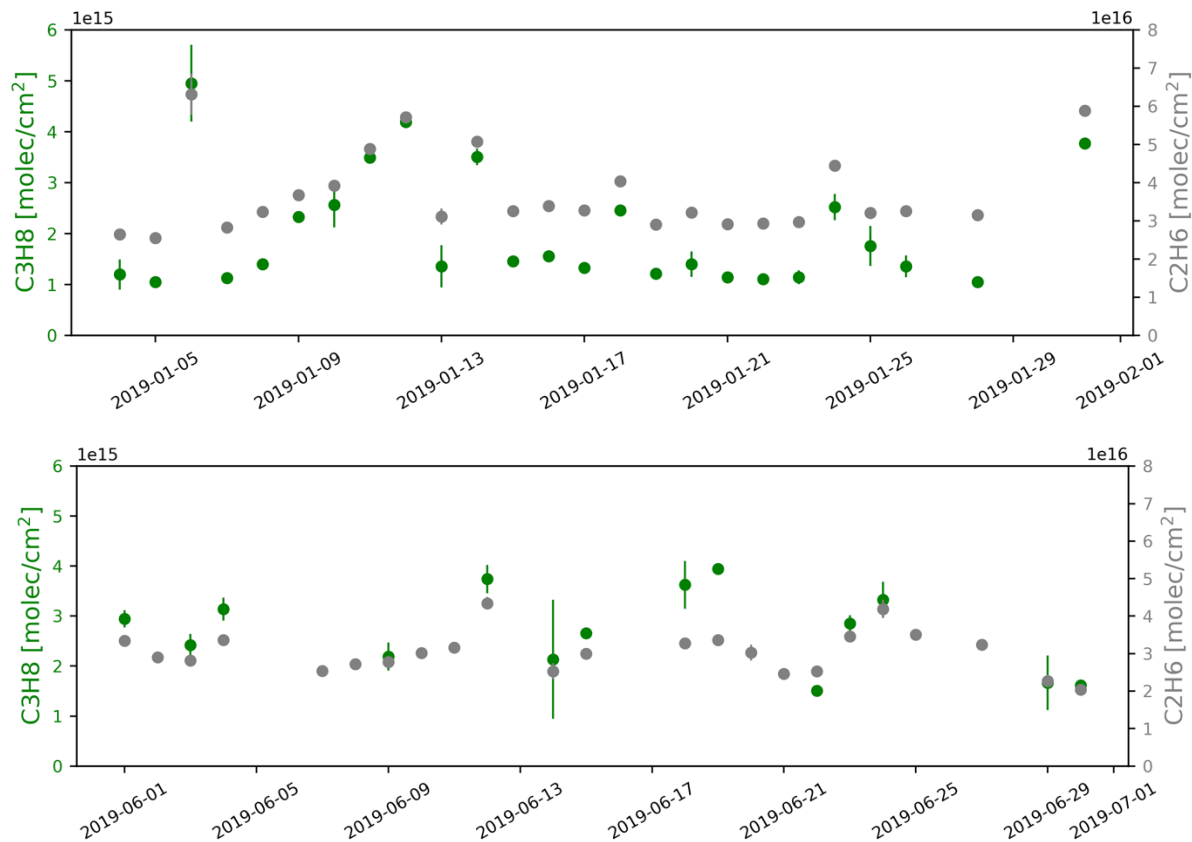
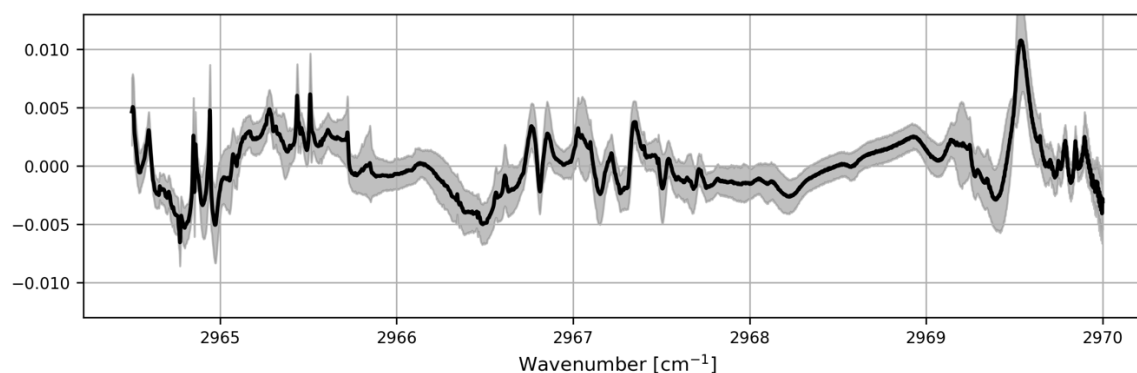


Figure A5. The time series of daily mean and SD of FTIR C3H8 and C2H6 measurements at Xianghe in January (upper panel) and June (bottom panel) 2019.

G2: Please discuss why the residual structure in Fig. 2 has structures that are larger than the ones found by Toon et al. (2021). Please present average spectral fit residuals in Fig. 2 (with std/min/max) to build confidence that your fit works. Are the average fit residuals understood?

**Thanks for the comment. The fit residuals in Fig.2 is from only 1 spectra (the spectra shown in Fig. 1), while the Fig.2 in Toon et al., (2021) shows the average of 5000 MKIV spectra. In the revised version, we added the mean and standard deviation of the fitting residuals from all 2783 C<sub>3</sub>H<sub>8</sub> retrievals at Xianghe. The mean RMS is 0.317%, which is slightly better than 0.3658% reported in Toon et al., (2021). In addition, the RMSE in Table 3 has been corrected. The original values in Table 3 are the values given by the SFIT4 code, which is RMSE/mean(y) but not RMSE. Mean(y) is the mean of the transmittance in this window. Now, we have recalculated the RMSE.**



**Figure A6. The mean (black line) and SD (grey shadow) of the fitting residual from 2783 FTIR C<sub>3</sub>H<sub>8</sub> retrievals at Xianghe between June 2018 and July 2022.**

Minor comments:

M1: You note the range of spectral resolution you have across the full MIR range. What is the spectral resolution in your window at ~2970 cm<sup>-1</sup>?

**The spectral resolution is 0.0051 cm<sup>-1</sup>. Added.**

M2: Page 4, lines 21-22: add C<sub>2</sub>H<sub>6</sub> to list of interfering gases

**Done.**

M3: the matrix  $S$  (not  $S_R$ ) on page 6, line 16 and in eq. 8 needs to be introduced in the text

**Added.**

M4: You calculate the retrieval error due to uncertainties in spectroscopic parameters, but did not include all relevant parameters like line position or line shift. Please explain why these can be neglected in the uncertainty budget.

**Thanks for the comment. In fact, we calculated all the model parameters, i.e. wavenumber shift, solar line intensity, solar line wavenumber shift, max optical path difference, instrument line shape, as the uncertainties derived from these parameters are less than 0.1%, they are not listed in Table 3.**

M5: How do you fit the spectral baseline (aka “background curvature”)? Please explain in the text.

**We use a linear regression ( $y=ax$ ) to fit the spectral baseline. The background slope is included in the state vector ( $x$ ). Since the retrieval window is relatively small of about  $5\text{ cm}^{-1}$ , we do not apply the second order fitting on the spectral background. Therefore, the background curvature is included in the model parameter vector ( $b$ ) but not retrieved.**

M6: Page 11, lines 14-19 and page 14, lines 14-16: Please provide a more convincing explanation why the C<sub>3</sub>H<sub>8</sub>-CH<sub>4</sub> correlation is weaker than the correlation with other NMHCs. There are oil and gas producing/consuming regions in Northern China (e.g. Changqing oil field/city of Beijing) and with a life time on the scale of weeks-months natural gas related C<sub>3</sub>H<sub>8</sub> emissions from such basins/cities could easily reach Xianghe (compare page 2, lines 20-23).

**Thanks for the comment. On one hand, according to the inventory, C<sub>3</sub>H<sub>8</sub> and C<sub>2</sub>H<sub>6</sub> are mainly emitted by oil and gas product, which is also a source of CH<sub>4</sub>. However, CH<sub>4</sub> has a multiply sources, and the major CH<sub>4</sub> emissions in North China are rice cultivation, waste, and animals instead of the oil and gas production. On the other band, CH<sub>4</sub> is a much longer lifetime as compared to C<sub>3</sub>H<sub>8</sub> and C<sub>2</sub>H<sub>6</sub>, therefore, CH<sub>4</sub> measurements includes the signal from a larger**

region as compared to C3H8 and C2H6 measurements. As a result, C3H8-CH4 correlation is weaker than the correlation with other NMHCs.

M7: How long is the integration time for one measurement?

**One measurement takes about 10 minutes.**

M8: I do not understand Fig. 9: why are there negative values for C3H8?

**Thanks for the comment. The negative values of C3H8 are from the MKIV retrievals based on the spectral fitting provided by Toon et al., (2021). As the negative values has no physical meaning, we have filtered them out in the revised version.**

M9: Is it possible that the C3H8 regularization is too loose?

**As the DOF of C3H8 is already close to 1.0 and the retrieved C3H8 vertical profile shape is similar to that of the a priori vertical profile shape, we believe that the C3H8 regularization is not loose. This is also true because of the weak absorption of C3H8. It is not possible to get too much vertical information from the observed spectra.**

M10: If differences between retrievals and a priori data are big: How trustworthy are the a priori profiles of C3H8 from WACCM and are they very different from the ones in CAMS? Would it not make sense to scale only the lower layers of the C3H8 profile, instead of fitting/scaling the full profile, especially since the retrieved profiles do not appear to differ substantially from the prior above ~10 km? How many layers are there below 10 km?

**The a priori columns are added in the Fig.5. We use the average WACCM model simulations between 1980 and 2040 as the a priori mole fraction profile, which does not vary with time. This fixed a priori profile is recommended by the NDACC-IRWG community. By doing this, we can reduce the impact from the prior.**

**There are 47 vertical layers between the surface and the top of the atmosphere (120 km) included in the SFIT4 code at Xianghe, with 15 layers below 10 km. The retrieved profiles also change above 10km. As the C3H8 mole fraction is very low above 10km, it is not so visible from the figure.**

M11: Which interfering species has the most impact on C3H8 retrieval accuracy/precision?

**H2O and CH4 have relatively large impacts on C3H8 retrieval. We have added the uncertainty estimation from these two interfering species in Table 3.**

M12: Have you checked the correlation between C3H8 and H2O/HDO? What did you find?

**See Figure A7. The correlation coefficient value between C3H8 and H2O columns is 0.5. In general, their correlation is not so significant.**

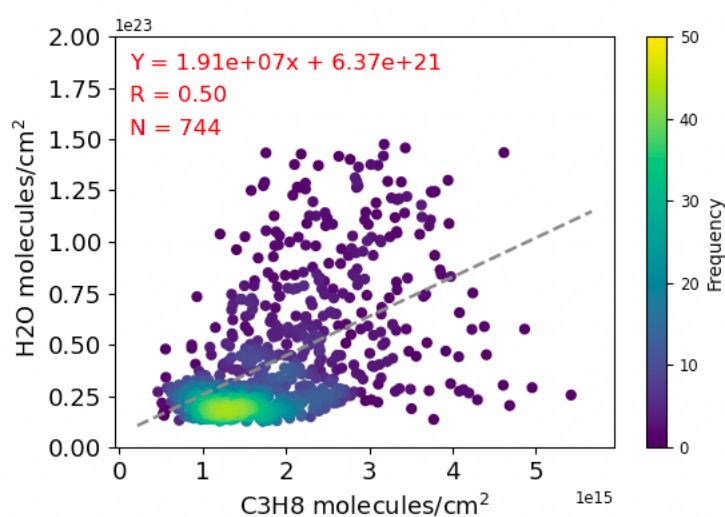


**Figure A7. The scatter plots between daily C3H8 and H2O columns at Xianghe.**

M13: Maybe mention somewhere that the DLR and HITRAN2020 line lists for H2O are very similar; I believe for the main isotopologue: HITRAN2020 = DLR, except for line positions, but better to double-check.

**Thanks for the comment. We have double-checked the line parameters in the HITRAN2020 and DLR in this window. They are similar, but still slightly different in both line position and line intensity. Table A1 shows an example of all the H2O main isotope (11) lines between 2965.5 and 2966.5 cm<sup>-1</sup> in these two line lists.**

**Table A1. All the H<sub>2</sub>O main isotope (11) lines between 2966.0 and 2966.5 cm<sup>-1</sup> in these two line lists.**

DLR		HITRAN2020	
wavenumber	Line intensity	wavenumber	Line intensity
2966.006188	1.63E-22	2966.006245	1.628E-22
2966.128478	6.88E-25	2966.068863	8.539E-30
		2966.457227	1.240E-30
		2966.480092	3.721E-30

Technical comments:

T1: page 2, line 4: “of the order of 10 years” -> “on the order of 10 years”

T2: caption of Table 1: “specie” -> “species”

T3: page 6, line 16 and caption of Table 3: 2040 -> 2004

T4: page 6, eq. 8:  $S_{ij}$  ->  $S_{\{ij\}}$

T5: page 7, line 13: pressure-dependent parameter, temperature-dependent parameter -> pressure-dependence parameter, temperature-dependence parameter

T6: page 10, line 17: “might due” -> “might be due”

T7: page 11, line 14: “separately(“ -> separately (“

T8: page 11, line 16: “have” -> “has”

T9: page 11, line 16: “it is probably due to that the” -> “it is probably due to the fact that the”

**Thanks. All the technique comments has been corrected.**

**References:**

**Pétron, G., et al. (2014), A new look at methane and nonmethane hydrocarbon emissions from oil and natural gas operations in the Colorado Denver-Julesburg Basin, J. Geophys. Res. Atmos., 119, 6836–6852, doi:10.1002/2013JD021272.**

# Atmospheric propane (C<sub>3</sub>H<sub>8</sub>) column retrievals from ground-based FTIR observations at Xianghe, China

Minqiang Zhou<sup>1</sup>, Pucai Wang<sup>1</sup>, Bart Dils<sup>2</sup>, Bavo Langerock<sup>2</sup>, Geoff Toon<sup>3</sup>, Christian Hermans<sup>2</sup>, Weidong Nan<sup>4</sup>, Qun Cheng<sup>4</sup>, and Martine De Mazière<sup>2</sup>

<sup>1</sup>Institute of Atmospheric Physics, Chinese Academy of Sciences, Beijing, China

<sup>2</sup>Royal Belgian Institute for Space Aeronomy (BIRA-IASB), Brussels, Belgium

<sup>3</sup>Jet Propulsion Laboratory, California Institute of Technology, Pasadena, CA, USA

<sup>4</sup>Xianghe Observatory of Whole Atmosphere, Institute of Atmospheric Physics, Chinese Academy of Sciences, Xianghe, China

**Correspondence:** Minqiang Zhou (minqiang.zhou@mail.iap.ac.cn); Pucai Wang (pcwang@mail.iap.ac.cn)

**Abstract.** Propane (C<sub>3</sub>H<sub>8</sub>) is an important trace gas in the atmosphere, as it is a proxy for oil and gas production and has a significant impact on atmospheric chemical reactions related to the hydroxyl radical and tropospheric ozone formation. In this study, solar direct absorption spectra near 2967 cm<sup>-1</sup> recorded by a ground-based Fourier Transform InfraRed spectrometer (FTIR) are applied to retrieve C<sub>3</sub>H<sub>8</sub> total columns between June 2018 and July 2022 at Xianghe in North China. The systematic and random uncertainties of the C<sub>3</sub>H<sub>8</sub> column retrieval are estimated to be ~~18.2~~18.4% and 18.1%, respectively. The mean and standard deviation of the C<sub>3</sub>H<sub>8</sub> columns derived from the FTIR spectra at Xianghe are 1.80±0.81(1σ) × 10<sup>15</sup> molecules/cm<sup>2</sup>. Good correlations are found between C<sub>3</sub>H<sub>8</sub> and other non-methane hydrocarbons, such as C<sub>2</sub>H<sub>6</sub> (R=0.84) and C<sub>2</sub>H<sub>2</sub> (R=0.79), as well as between C<sub>3</sub>H<sub>8</sub> and CO (R=0.72). However, the correlation between C<sub>3</sub>H<sub>8</sub> and CH<sub>4</sub> is relatively weak (R=0.45). The Moreover, the FTIR C<sub>3</sub>H<sub>8</sub> measurements at Xianghe are also compared against ~~two atmospheric chemical transport model simulations (the Whole Atmosphere Community Climate Model (WACCM) and the Copernicus Atmosphere Monitoring Service (CAMS)). We find that the C<sub>3</sub>H<sub>8</sub> columns from both models have different seasonal variations as compared to the FTIR measurements. Moreover, the mean C<sub>3</sub>H<sub>8</sub> columns derived from the WACCM and CAMS models are about 68% larger than the FTIR retrievals~~MKIV measurements at several sites around the world. The new FTIR measurements at Xianghe provide us an insight into the C<sub>3</sub>H<sub>8</sub> column variations and underlying processes in North China.

## 15 1 Introduction

Methane (CH<sub>4</sub>) and non-methane hydrocarbons (NMHC), such as ethane (C<sub>2</sub>H<sub>6</sub>), acetylene (C<sub>2</sub>H<sub>2</sub>), propane (C<sub>3</sub>H<sub>8</sub>), propene (C<sub>3</sub>H<sub>6</sub>), and isoprene (C<sub>5</sub>H<sub>8</sub>), are important trace gases that play significant roles in atmospheric chemical reactions related to hydroxyl radical (OH) abundance and tropospheric ozone (O<sub>3</sub>) formation (Sze, 1977; Donahue and Prinn, 1990; Tan et al., 2012; Lelieveld et al., 2015). Human activities contribute greatly to the emissions of CH<sub>4</sub> and NMHCs, especially in urban areas (Bourtsoukidis et al., 2019; Saunois et al., 2020). Atmospheric C<sub>2</sub>H<sub>6</sub> and C<sub>3</sub>H<sub>8</sub> emissions are dominated by oil and



gas sources, and they are co-emitted with CH<sub>4</sub>. Therefore, numerous studies used the ratio of C<sub>2</sub>H<sub>6</sub> and/or C<sub>3</sub>H<sub>8</sub> to CH<sub>4</sub> to understand the CH<sub>4</sub> trend (Kort et al., 2016; Franco et al., 2016; Rigby et al., 2017).

The major sink of C<sub>2</sub>H<sub>6</sub> and C<sub>3</sub>H<sub>8</sub> is the reaction with OH, and the lifetime of C<sub>3</sub>H<sub>8</sub> and C<sub>2</sub>H<sub>6</sub> is about 2-4 weeks in summer and 2 months in winter (Jacob, 1999; Xiao et al., 2008). Compared to CH<sub>4</sub> with a lifetime ~~of the~~ on an order of 10 years (IPCC, 2013), the short-lived gases C<sub>2</sub>H<sub>6</sub> and C<sub>3</sub>H<sub>8</sub> are not well-mixed on the global scale, and are therefore more representative of regional pollution as is carbon monoxide (CO) (Toon et al., 2021).

Atmospheric C<sub>3</sub>H<sub>8</sub> concentrations at the surface are observed by National Oceanic and Atmospheric Administration (NOAA) - Global Monitoring Laboratory (GML) flask sampling measurements at 12 sites (<https://gml.noaa.gov/hats/gases/C3H8.html>). In addition, the HIPER Pole-to-Pole Observations (HIPPO), Atmospheric Tomography (ATom), and In-service Aircraft for a Global Observing System (IAGOS) aircraft campaigns provide in-situ gas analyzer measurements of C<sub>3</sub>H<sub>8</sub> with a wide latitudinal coverage, particularly in the Pacific Ocean, Atlantic Ocean, Europe and North America (Wofsy, 2011; Thompson et al., 2022; Li et al., 2022). Toon et al. (2021) has demonstrated the use of C<sub>3</sub>H<sub>8</sub> absorption lines in the mid-infrared region (Harrison et al., 2010), in solar absorption spectra from MkIV interferometers for retrieving the C<sub>3</sub>H<sub>8</sub> total columns or vertical profiles at several locations in Sweden, the USA, and Antarctica. Solar absorption infrared spectra are also being collected by ground-based Fourier Transform Spectrometers (FTIR) within the Network for the Detection of Atmospheric Composition Change - InfraRed Working Group (NDACC-IRWG) (De Mazière et al., 2018). Currently, there are more than 20 NDACC-IRWG global sites, with a good global latitudinal coverage from 78°S to 80°N (<https://www2.acom.ucar.edu/irwg/sites>). However, to our knowledge, no site has reported C<sub>3</sub>H<sub>8</sub> retrievals from spectra observed by a Bruker 125HR spectrometer within the NDACC-IRWG.

Xianghe (39.75 °N, 116.96 °E) is located in North China, about 50 km east of the mega-city Beijing (Yang et al., 2020). According to the Emissions Database for Global Atmospheric Research (EDGAR) v6.0 (Crippa et al., 2020) and the Multi-resolution Emission Inventory for China (MEIC) inventory (Wang et al., 2015; Li et al., 2017), there is a large CH<sub>4</sub> emission source in North China coming from fuel exploitation and oil refineries. Therefore, we expect that the C<sub>2</sub>H<sub>6</sub> and C<sub>3</sub>H<sub>8</sub> concentrations are relatively high in this region. In June 2018, a Bruker IFS 125HR spectrometer, compliant with the NDACC-IRWG protocol, started recording solar absorption spectra in the mid-infrared spectral range. The spectra have been used to retrieve several atmospheric components, e.g., O<sub>3</sub>, CH<sub>4</sub>, CO, C<sub>2</sub>H<sub>2</sub>, C<sub>2</sub>H<sub>6</sub>, HCN and H<sub>2</sub>CO (Ji et al., 2020; Zhou et al., 2020, 2021, 2023; Vigouroux et al., 2020; Sha et al., 2021). In this study, we investigate the C<sub>3</sub>H<sub>8</sub> retrieval from ground-based FTIR spectra at Xianghe, and discuss the C<sub>3</sub>H<sub>8</sub> column variation in North China, based on these new FTIR measurements.

The remainder of this paper is organized as follows. Section 2 describes the Xianghe FTIR site and C<sub>3</sub>H<sub>8</sub> retrieval method, Section 3 presents the C<sub>3</sub>H<sub>8</sub> variations and correlations with other species. Moreover, the C<sub>3</sub>H<sub>8</sub> measurements at Xianghe are compared to ~~model simulations and~~ ground-based MkIV measurements at other places. Finally, Section 4 draws a conclusion.

## 2 Method

### 2.1 Xianghe FTIR spectra measurement

The Xianghe FTIR measurement system started in June 2018, and has been well described in previous studies (Yang et al., 2020; Zhou et al., 2021, 2023). Briefly, the FTIR measurement system contains 3 parts: a solar tracker system, a weather station, and a Bruker IFS 125HR Fourier-transform infrared (FTIR) spectrometer. Short-Wave infrared (SWIR) and Near-infrared (NIR) spectra ( $4000\text{-}11000\text{ cm}^{-1}$ ) with a spectral resolution of  $0.02\text{ cm}^{-1}$  are recorded with an InGaAs detector, and these spectra are used to derive greenhouse gases total column abundances as a contribution to the Total Carbon Column Observing Network (TCCON). Mid-infrared (MIR) spectra ( $1800\text{-}4500\text{ cm}^{-1}$ ), with a spectral resolution of  $0.0035\text{-}0.0070\text{ cm}^{-1}$ , are recorded with an InSb detector. To enhance the signal-to-noise ratio (SNR) of the spectra, we add specific optical filters into the light path when recording each MIR spectrum as recommended by NDACC-IRWG (Blumenstock et al., 2021; Zhou et al., 2023). A typical MIR spectrum, with a spectral resolution of  $0.0051\text{ cm}^{-1}$ , used for  $\text{C}_3\text{H}_8$  retrieval is shown in Figure 1. Note that, we only operate the FTIR measurement during the daytime and under clear-sky conditions, as the sun is the light source. In general, we carry out 4 to 10 MIR spectral measurements of this type per day for about 200 days per year. Each spectrum takes about 10 minutes to record. The spectra taken between June 2018 and July 2022 (about 4 years) are used in this study.

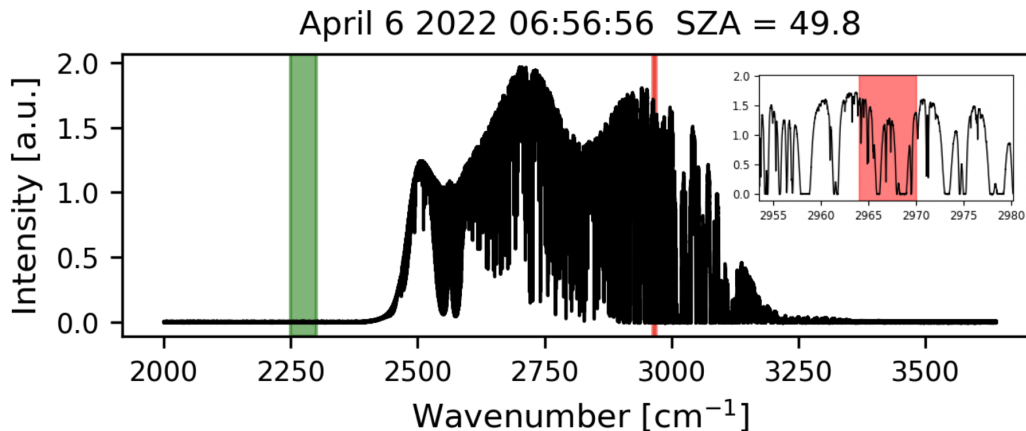


**Figure 1.** A typical MIR spectrum observed at Xianghe on 6 April 2022 with a solar zenith angle of  $49.8^\circ$ . The red and green windows indicate the micro-windows windows used for the  $\text{C}_3\text{H}_8$  retrieval and for calculating the noise (Eq. 5), respectively. The insert in the right-hand corner shows a zoom on the retrieval micro-window.

### 2.2 Retrieval method

To derive  $\text{C}_3\text{H}_8$  mole fractions from the observed spectra, we follow the optimal estimation methodology (Rodgers, 2000). The forward model ( $\mathbf{F}$ ) simulates the absorption spectra ( $\mathbf{y}$ ) observed by the FTIR system. It includes modelling of the solar

spectra at the top of the atmosphere (TOA), the physics of the radiative transfer from the TOA to the ground-based FTIR, and the FTIR spectrometer line shape function (ILS). Then, the observed spectra ( $\mathbf{y}$ ) can be written as

$$\mathbf{y} = \mathbf{F}(\mathbf{x}, \mathbf{b}) + \epsilon, \quad (1)$$

where  $\mathbf{x}$  is the state vector (retrieved parameters),  $\mathbf{b}$  is the forward model parameters (not retrieved), and  $\epsilon$  is the error, including the measurement noise and forward model errors. We wish to find the optimal state ( $\mathbf{x}$ ) that minimize the cost function ( $\mathbf{J}(\mathbf{x})$ ), given by

$$\mathbf{J}(\mathbf{x}) = [\mathbf{y} - \mathbf{F}(\mathbf{x})]^T \mathbf{S}_\epsilon^{-1} [\mathbf{y} - \mathbf{F}(\mathbf{x})] + [\mathbf{x} - \mathbf{x}_a]^T \mathbf{S}_R [\mathbf{x} - \mathbf{x}_a], \quad (2)$$

where  $\mathbf{S}_\epsilon$  is the measurement error covariance matrix;  $\mathbf{S}_R$  is the regularization matrix;  $\mathbf{x}_a$  is the *a priori* state vector. The Levenberg-Marquardt (LM) method is used to iteratively solve the above equation:

$$\mathbf{x}_{i+1} = \mathbf{x}_i + [(1 + \gamma)\mathbf{S}_R + \mathbf{K}_i^T \mathbf{S}_\epsilon^{-1} \mathbf{K}_i]^{-1} \{ \mathbf{K}_i^T \mathbf{S}_\epsilon^{-1} [\mathbf{y} - \mathbf{F}(\mathbf{x}_i)] - \mathbf{S}_R [\mathbf{x}_i - \mathbf{x}_a] \}, \quad (3)$$

where  $\mathbf{K}$  is the Jacobian matrix,  $\gamma$  is a parameter to adjust the regularization of a priori information in each iteration step (Rodgers, 2000). Upon convergence, the final state is called  $\mathbf{x}_r$ , which can be related to the true state ( $\mathbf{x}_t$ ):

$$\mathbf{x}_r = \mathbf{x}_a + \mathbf{A}(\mathbf{x}_t - \mathbf{x}_a) + \epsilon, \quad (4)$$

where  $\mathbf{A}$  is the averaging kernel matrix, representing the sensitivity of the retrieved parameters to the true parameter, and  $\epsilon$  is the retrieval uncertainty propagated from Eq.1.

### 2.3 Retrieval strategy

In this study, we use the SFIT4 v1.0 retrieval algorithm (Pougatchev et al., 1995; Hase et al., 2004) to perform the forward model simulation as well as the LM inversion. The well-established SFIT4 code has been used extensively to retrieve total/partial column of atmospheric species in the NDACC-IRWG community (Zhou et al., 2016; De Mazière et al., 2018; Ortega et al., 2019).

The key  $\text{C}_3\text{H}_8$  retrieval parameters used in this study are listed in Table 1. The retrieval window is set to 2964.5-2970.0  $\text{cm}^{-1}$ , where we have the strongest  $\text{C}_3\text{H}_8$  absorption line (Harrison et al., 2010). Apart from  $\text{C}_3\text{H}_8$ , several interfering gases ( $\text{H}_2\text{O}$ ,  $\text{CH}_4$ ,  $\text{O}_3$ ,  $\text{C}_2\text{H}_6$  and HDO) also have absorption lines in this window as shown in Figure 2. To reduce the impact of uncertainties about the abundances of these species, ~~these column abundances~~  $\text{CH}_4$ ,  $\text{O}_3$ ,  $\text{C}_2\text{H}_6$ , and HDO columns are retrieved along with the target gas mole fractions; ~~only for~~. For these three species, their profile shapes are fixed and only the scaling factors are retrieved. As  $\text{H}_2\text{O}$  absorption lines are strong (Table 1) and  $\text{H}_2\text{O}$  variability are relatively large in the atmosphere, we perform a profile retrieval ~~, because of its large variability~~ for  $\text{H}_2\text{O}$ . The state vector includes  $\text{CH}_4$ ,  $\text{O}_3$ ,  $\text{C}_2\text{H}_6$ , and HDO columns, as well as 47-layers'  $\text{C}_3\text{H}_8$  and  $\text{H}_2\text{O}$  mole fractions.

The chosen spectroscopic parameters are crucial in the remote sensing technique. In this study, we have tested several line lists, particularly for  $\text{H}_2\text{O}$  (HDO) and  $\text{CH}_4$  (see Table 2), including DLR2016 (Loos et al., 2017), HITRAN2020 (Gordon et al.,

2022) and ATM2020 (<https://mark4sun.jpl.nasa.gov/pseudo.html>). The ATM2020 line list is created by Geoff Toon (NASA, JPL) based on HITRAN2020 together with some additional atmospheric and laboratory measurements. It includes pseudo line lists (PLL) for certain species as the ones we use for C<sub>3</sub>H<sub>8</sub>, based on laboratory cross section measurements by Harrison et al. (2010). For C<sub>2</sub>H<sub>6</sub>, we use HITRAN2020. We tested more than 1000 spectra recorded in 2019 at Xianghe, and we observed that the lowest root-mean-square error (RMSE) of the fitting residual is obtained when the ATM2020 spectral database is used for CH<sub>4</sub> and H<sub>2</sub>O. Table 1 lists the spectral datasets finally used for each species in the C<sub>3</sub>H<sub>8</sub> retrieval strategy.

**Table 1.** The retrieval window, interfering species, spectroscopy, fitting parameters for C<sub>3</sub>H<sub>8</sub> at Xianghe.

Parameters	settings
Retrieval window (cm <sup>-1</sup> )	2964.5-2970.0
Profile retrieval species	C <sub>3</sub> H <sub>8</sub> , H <sub>2</sub> O
Column retrieval species	C <sub>2</sub> H <sub>6</sub> , CH <sub>4</sub> , HDO
Retrieved parameters	slope, phase, instrument line shape, wavenumber shift solar intensity, solar wavenumber shift
A priori profile	NCEP for H <sub>2</sub> O, HDO; WACCM for C <sub>2</sub> H <sub>6</sub> , C <sub>3</sub> H <sub>8</sub> , CH <sub>4</sub>
Spectroscopy	PLL for C <sub>3</sub> H <sub>8</sub> ; ATM20 for H <sub>2</sub> O, HDO, CH <sub>4</sub> ; HITRAN2020 for C <sub>2</sub> H <sub>6</sub>
Regularization	Tikhonov L <sub>1</sub> method
DOFS	1.1

**Table 2.** The fitting RMSE of the retrieval window for all spectra in 2019 from several different line lists.

H <sub>2</sub> O (HDO)	CH <sub>4</sub>	RMSE (mean ± 1σ)
ATM2020	ATM2020	0.9250.313 ± 0.2410.081
HITRAN2020	ATM2020	0.9670.327 ± 0.2670.091
DLR	ATM2020	0.9680.328 ± 0.2670.091
ATM2020	HITRAN2020	1.2330.417 ± 0.2810.095
HITRAN2020	HITRAN2020	1.3140.445 ± 0.2890.097

The *a priori* profiles for C<sub>3</sub>H<sub>8</sub>, C<sub>2</sub>H<sub>6</sub>, and CH<sub>4</sub> are derived from the Whole Atmosphere Community Climate Model (WACCM) version 6. We use the averages of the monthly means between 1980 and 2040 (61 years) as the *a priori* profiles. Since the variations of temperature and humidity are quite large in the atmosphere, using fixed *a priori* profiles often results in a bad fitting, especially for the first iteration. To provide a better estimation of temperature and humidity profiles, for each measurement, the H<sub>2</sub>O (HDO) and temperature vertical profiles are derived from the closest 6-hourly NCEP reanalysis data (Saha et al., 2014), and linearly interpolated to the measurement time.

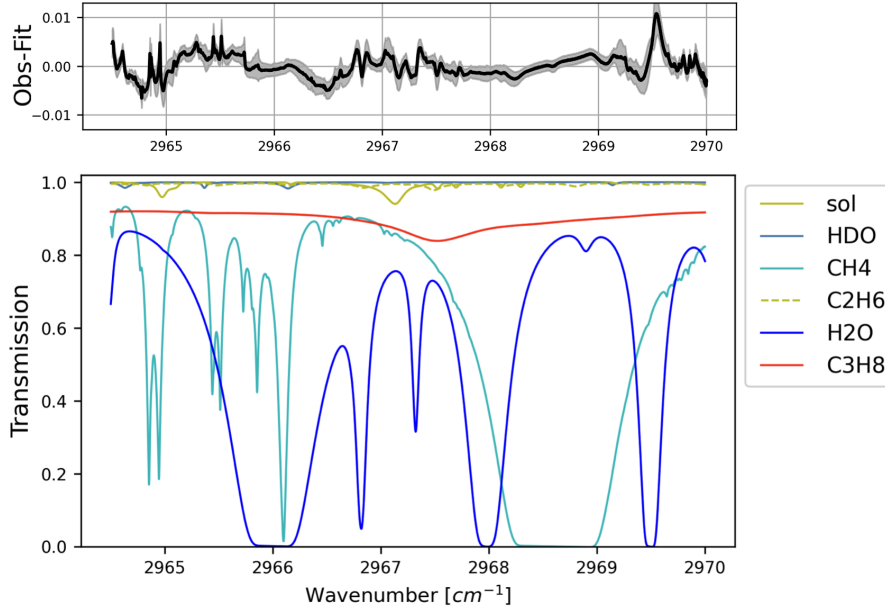


**Figure 2.** The transmittances of main species and solar lines (bottom), as well as the fitting residual (top) using the typical spectrum shown in Figure 1 in this retrieval window mean (black line) and standard deviation (grey shadow) from all 2783 FTIR C3H8 retrievals at Xianghe between June 2018 and July 2022. The mean RMSE is 0.317%.

According to Eq.2, the cost function  $J(x)$  is composed of the measurement and *a priori* information, each contracted with a weight matrix  $S_\epsilon$  and  $S_R$ , respectively. In this study, the diagonal of the  $S_\epsilon$  is calculated as  $1/\text{SNR}^2$ , and the non-diagonal values are set to 0. The SNR is calculated as

$$\text{SNR} = \frac{\overline{I_r}}{\sigma_{I_n}}, \quad (5)$$

- 5 where  $\overline{I_r}$  is the max radiation intensity in the  $\text{C}_3\text{H}_8$  retrieval window ( $2964.5\text{-}2970.0 \text{ cm}^{-1}$ ; red window in Figure 1) and  $\sigma_{I_n}$  is the standard deviation (std) of the intensity in the noise window ( $2250.0\text{-}2300.0 \text{ cm}^{-1}$ ; green window in Figure 1). The Tikhonov  $L_1$  regularization method (Tikhonov, 1963) is applied to generate the  $S_R$ , with

$$S_R = \alpha L_1^T L_1, \quad (6)$$

$$L_1 = \begin{bmatrix} -1 & 1 & 0 & \dots & 0 & 0 \\ 0 & -1 & 1 & \dots & 0 & 0 \\ \vdots & \vdots & \vdots & \ddots & \vdots & \vdots \\ 0 & 0 & 0 & \dots & -1 & 1 \end{bmatrix}. \quad (7)$$

- 10 To determine the  $\alpha$  value in Eq. 6, we apply the degree of freedom for signal (DOF) method proposed by Steck (2002). The trace of the averaging kernel matrix ( $\mathbf{A}$ ) is the DOF, indicating the pieces of independent information of the retrieval (Rodgers,

2000). First, we use the optimal estimation method (OEM) to get an estimated DOF.  ~~$\mathbf{S}_R$  using the OEM is~~ Using the OEM method,  $\mathbf{S}_R = \mathbf{S}_a^{-1}$ , where  $\mathbf{S}_a$  is the a priori covariance matrix, which is derived from a covariance matrix on the WACCM monthly means between 1980 and 2040 ( $\mathbf{S}_{R_{i,i}} = \mathbf{S}_{i,i}^{-1} = \sigma_i^{-2}$  ( $\mathbf{S}_R)_{i,i} = (\mathbf{S}_a)_{i,i}^{-1} = \sigma_i^{-2}$ ; diagonal values), and the non-diagonal values are set as

$$5 \quad \underline{\mathbf{S}_{R_{i,j}}^{-1} = \mathbf{S}_{i,j} = e^{(d_{i,j}/4)} / (\sigma_i \sigma_j)},$$

( $\mathbf{S}_R)_{i,j} = (\mathbf{S}_a)_{i,j}^{-1} = (\sigma_i \sigma_j) / e^{(d_{i,j}/4)}$ , where  $d_{i,j}$  is the vertical distance between layer  $i$  and layer  $j$ , in km. The DOF derived from the OEM is about 1.1, indicating that there is only column information for the  $\text{C}_3\text{H}_8$  retrieval. Knowing that, we tune the  $\alpha$  value in Eq.6 to make the DOF derived from the Tikhonov method close to the DOF that is derived from the OEM; this approach results in setting  $\alpha$  to 1000.

## 10 2.4 Retrieval uncertainty

The retrieval error ( $\epsilon$ ) of the FTIR  $\text{C}_3\text{H}_8$  column contains three parts as

$$(\mathbf{A} - \mathbf{I})(\mathbf{x}_t - \mathbf{x}_a) \quad \dots \quad \text{smoothing error} \quad (8)$$

$$\mathbf{G}_y \mathbf{K}_b (\mathbf{b}_t - \mathbf{b}_a) \quad \dots \quad \text{model parameter error} \quad (9)$$

$$\mathbf{G}_y \epsilon \quad \dots \quad \text{measurement error} \quad (10)$$

15 where  $\mathbf{G}_y$  is the contribution function;  $\mathbf{b}_t$  and  $\mathbf{b}$  are the true and used model inputs, respectively. Table 3 lists the systematic and random uncertainty of each component. The vertical distributions of the systematic and random uncertainties are shown in Figure 3. For the smoothing error, we separate the contributions into target species ( $\text{C}_3\text{H}_8$ ), interfering species ( $\text{H}_2\text{O}$ ,  $\text{HDO}$ ,  $\text{CH}_4$ ,  $\text{C}_2\text{H}_6$ ), and retrieved parameters (slope, phase, wavenumber shift, instrument line shape, solar intensity and shift). For the model parameter contributions, we calculate the  $\text{C}_3\text{H}_8$  uncertainty contribution coming from spectroscopy, solar zenith angle  
20 (SZA), temperature profile, curvature parameter, and zero level shift (zshift). Since  $\text{CH}_4$  and  $\text{H}_2\text{O}$  have stronger absorptions than  $\text{C}_3\text{H}_8$ , and their absorption lines are not perfectly fitted, the impact from the spectroscopy uncertainty of  $\text{CH}_4$  and  $\text{H}_2\text{O}$  are calculated as well.

The systematic and random uncertainties of each parameter are also listed in Table 3. ~~The vertical distributions of the systematic and~~ It is assumed that 10% of the a priori profile is used to derive the diagonal values of the systematic covariance matrix ( $\mathbf{S}_a)_{i,i}^{sys} = \sigma_i^2$ , and the off-diagonal values of  $\mathbf{S}_a^{sys}$  are calculated as ( $\mathbf{S}_a)_{i,j}^{sys} = \sigma_i \sigma_j$  (von Clarmann, 2014). The covariance matrix derived from the WACCM 61-years' monthly means are set to the random covariance matrix  $\mathbf{S}_a^{ran}$ . Regarding the model parameter uncertainties in the Table 3, the systematic/random ~~uncertainties are shown in Figure 3.~~  $\mathbf{S}_b$  matrix is created by the mean and standard deviation of the differences between NCEP and ERA5 at Xianghe. The random deviation is about 2 K, and the systematic deviation is about 1.5 K for the whole vertical range. For the target spectroscopic parameters, the relative uncertainties of  $\text{C}_3\text{H}_8$  is set to 4% according to the pseudo database. For the  $\text{CH}_4$  and  $\text{H}_2\text{O}$  spectroscopy parameters, the relative uncertainty of 5% is derived from the HITRAN2020 dataset (Gordon et al., 2022). Note that the spectroscopy uncertainty in  
30

Table 3 is the sum of the uncertainties from the line intensity, ~~pressure-dependent~~ pressure dependent parameter (linePAir) and ~~temperature-dependent~~ temperature dependent parameter (lineTAir). For the uncertainties of background curvature, zero offset (shift), and SZA, we use the default values provided by the SFIT4 algorithm (<https://wiki.ucar.edu/display/sfit4/SFIT4+Version+1.0.xx+Release>), which are recommended by the NDACC-IRWG community.

- 5 Based on our uncertainty estimation, the total systematic and random uncertainty of the C<sub>3</sub>H<sub>8</sub> column are both about 18%, and the dominating contribution is the uncertainty on the background curvature parameter in the forward model. To represent the variability of the C<sub>3</sub>H<sub>8</sub>, we select all days with at least 3 individual measurements on each day, and calculate the daily std. The average of all the daily stds is about 15.3%, and it is close to our estimated random uncertainty.

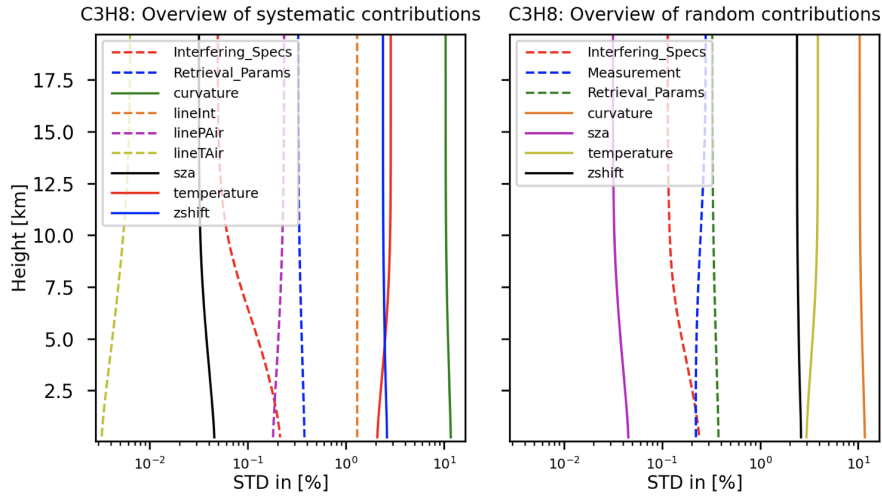
**Table 3.** The systematic and random (sys/ran) retrieval uncertainties for the total columns of C<sub>3</sub>H<sub>8</sub>. The '-' means that the uncertainty is less than 0.1%. 1  $\sigma$  of the target or interfering species is the std derived from the WACCM model monthly means between 1980 and 2040. The relative std in the bottom row is the average of daily std of C<sub>3</sub>H<sub>8</sub> columns on all days with at least 3 measurements, which is to represent the variability of the retrieval.

Error source	Parameter	Parameter uncertainty (sys/ran)	C <sub>3</sub> H <sub>8</sub> column uncertainty [%]
Smoothing error	Target species ( <u>C<sub>3</sub>H<sub>8</sub></u> )	10/1 $\sigma$ %	0.2/0.5
	Interfering species ( <u>H<sub>2</sub>O, CH<sub>4</sub>, HDO, C<sub>2</sub>H<sub>6</sub></u> )	10/1 $\sigma$ %	0.7/0.6
	Retrieved parameters		0.6/0.6
Model parameter error	Spectroscopy <u>for C<sub>3</sub>H<sub>8</sub></u>	4.0/- %	4.1/-
	<u>Spectroscopy for H<sub>2</sub>O and CH<sub>4</sub></u>	<u>5.0/- %</u>	<u>2.5/-</u>
	SZA	0.03/0.03°	0.1/0.1
	Curvature	0.1/0.1 %	17.2/17.2
	Temperature	1.5/2.0 K	2.7/3.9
	Zshift	0.15/0.15 %	2.9/2.9
Measurement error		$-\frac{1}{\text{SNR}}$	-/1.0
Total			<del>18.2</del> <u>18.4</u> /18.1
Std			-/15.3

### 3 Results and discussions

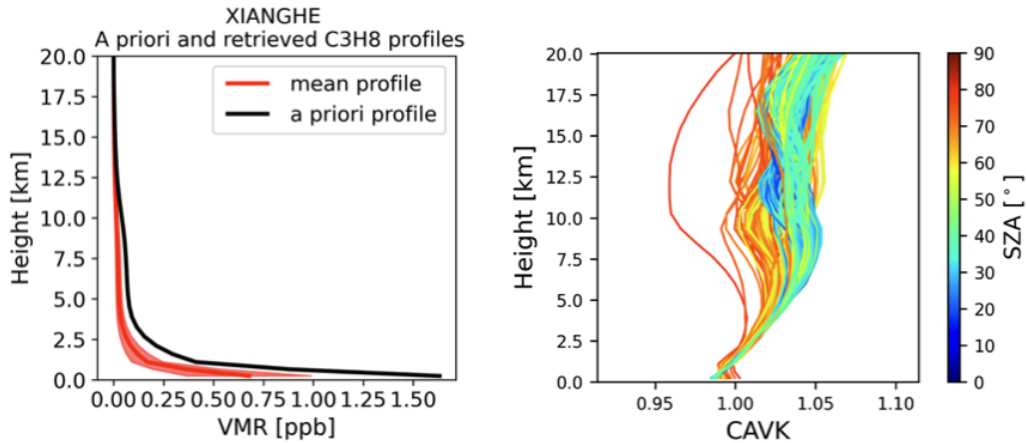
#### 10 3.1 FTIR C<sub>3</sub>H<sub>8</sub> retrievals at Xianghe

Figure 4 shows the *a priori* profile and retrieved profiles of C<sub>3</sub>H<sub>8</sub>. The vertical profile of C<sub>3</sub>H<sub>8</sub> from the WACCM model shows that the C<sub>3</sub>H<sub>8</sub> mole fraction is high near the surface and decreases with increasing altitude. Such a vertical shape is expected as the C<sub>3</sub>H<sub>8</sub> emissions are at the surface, and its atmospheric lifetime is too short to achieve a well-mixed troposphere. Although



**Figure 3.** The vertical profiles of the systematic (left) and random error (right) of the FTIR  $C_3H_8$  retrieval from each component.

we perform a profile retrieval on  $C_3H_8$ , we only have about 1 DOF. In addition, the Tikhonov regularization matrix constrains the vertical shape when the DOF is typically close to 1.0. As a result, the retrieved  $C_3H_8$  profiles have a very similar vertical shape as the *a priori* profile. However, the FTIR measurements show that the *a priori* column overestimates the  $C_3H_8$  column concentration by about 100%. The column averaging kernel indicates the sensitivity of the retrieved  $C_3H_8$  column to the  $C_3H_8$  partial column in each height. Figure 4 shows that the retrieved  $C_3H_8$  column has good sensitivity to all the layers, and slightly varies with SZA.



**Figure 4.** The *a priori* and retrieved  $C_3H_8$  profiles (left), and the column averaging kernel (CAVK) varying with SZA (right).



The time series and seasonal variation of FTIR  $C_3H_8$  column measurements are presented in Figure 5. To better visualize the seasonal variation, the column measurements are fitted by a periodic function  $y(t) = A_0 + \sum_{k=1}^3 (A_{2k-1} \cos(2k\pi t) + A_{2k} \sin(2k\pi t))$ , where  $A_0$  is the offset, and  $A_1$  to  $A_6$  are the periodic amplitudes, representing the seasonal variation. The obtained mean and std of  $C_3H_8$  columns at Xianghe are  $1.80 \pm 0.81 \times 10^{15} \text{ molec./cm}^2$ . The  $C_3H_8$  columns show a high mean value in July and a low value in October. The difference between the median values in July (maximum) and October (minimum) is  $1.2 \times 10^{15} \text{ molec./cm}^2$ . Although the median values of  $C_3H_8$  columns in June-August are larger than those in October-March, we notice that extremely high  $C_3H_8$  columns often occur in the latter period.

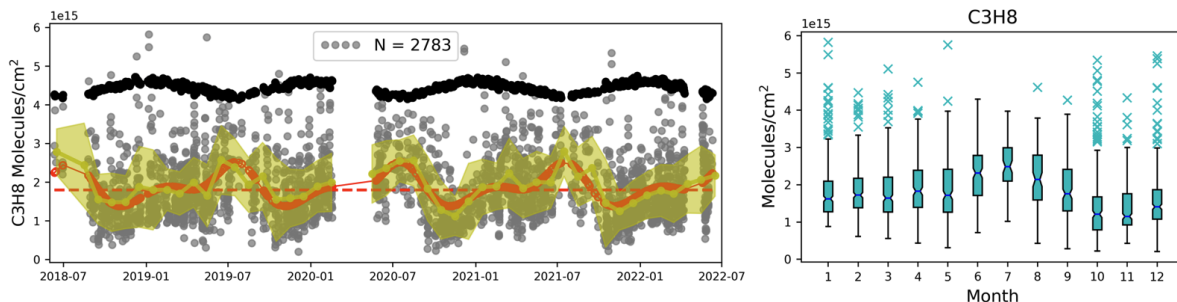


**Figure 5.** Left panel shows the time series of FTIR individual  $a$  priori  $C_3H_8$  column measurements (black dots), retrieved columns (grey dots), monthly means (yellow line), monthly stds (yellow shade), periodic function fitting (red solid line) and the fitted offset (red dashed line). Right panel: the monthly box plot of the  $C_3H_8$  columns. The bottom and top bars represent the 10% and 90% percentiles of the datasets and the blue crosses are the extremely high values above 90%.

### 3.2 FTIR $C_3H_8$ measurements against model simulations

In this section, we compare the FTIR  $C_3H_8$  measurements at Xianghe with two well-known global atmospheric chemistry transport models: WACCM and Copernicus Atmosphere Monitoring Service (CAMS). The WACCM model has been widely used to generate *a priori* profiles in the NDACC-IRWG community, spanning an altitude range from the Earth's surface to the thermosphere (Marsh et al., 2013; Gettelman et al., 2019). The horizontal resolution of the WACCM is  $0.95^\circ \times 1.25^\circ$ , with 70 vertical levels from the surface to 120 km. More information about the WACCM v6 model can be found in . The CAMS model (EAC4) is the fourth generation ECMWF global reanalysis of atmospheric composition, which combines model data with observations across the world. The horizontal resolution of the CAMS is  $0.75^\circ \times 0.75^\circ$ , with 60 model levels from the surface to  $\sim 0.1$  hPa. For more information about the CAMS model, we refer to Inness et al. (2019).

Figure 6 shows the monthly  $C_3H_8$  column distributions derived from FTIR measurements, the WACCM model, and the CAMS model at Xianghe between June 2018 and December 2022. The mean and std of  $C_3H_8$  column derived from CAMS and WACCM are  $3.07 \pm 1.37 \times 10^{15} \text{ molec./cm}^2$ , and  $3.00 \pm 1.08 \times 10^{15} \text{ molec./cm}^2$ , respectively. The mean  $C_3H_8$  columns from CAMS and WACCM models are similar, but both models are about 68% larger than the FTIR measurement. The mean difference between the model and FTIR  $C_3H_8$  column is larger than the systematic uncertainty of the FTIR retrieval ( $\sim 18\%$ ).

Moreover, the seasonal variations of  $C_3H_8$  columns derived from the CAMS and WACCM models are different from the one derived from the FTIR measurements. CAMS and WACCM both show a low  $C_3H_8$  column in summer, when the FTIR measurements present the maximum median  $C_3H_8$  column. The seasonal variation of  $C_3H_8$  at JPL (34°N) derived from the ground-based MKIV spectrometer also observes a high value in summer (Toon et al., 2021), which is similar to the  $C_3H_8$  seasonal variation derived from the FTIR measurements at Xianghe (39°N). Such a difference in seasonal variation between the FTIR measurements and model simulations might due to the uncertainty of emissions, transports, chemical reactions, and sinks.

The monthly box plot of the  $C_3H_8$  columns derived from the CAMS model, the WACCM model, and the FTIR measurements at Xianghe between June 2018 and December 2021.

### 3.2 Correlations with CO, CH<sub>4</sub>, C<sub>2</sub>H<sub>2</sub> and C<sub>2</sub>H<sub>6</sub> at Xianghe

As mentioned above, the infrared spectra observed by the Xianghe FTIR system have been also used to retrieve CO, CH<sub>4</sub>, C<sub>2</sub>H<sub>2</sub> and C<sub>2</sub>H<sub>6</sub> columns using NDACC-IRWG recommended retrieval recipes (Ji et al., 2020; Zhou et al., 2023), which allows us to investigate the correlation between  $C_3H_8$  and these species. We are particularly interested in the correlation on a regional scale. Therefore, to reduce the impact from the background, we calculate the  $\Delta_{\text{gas}}$  ( $\Delta_{\text{gas}} = \text{gas} - \text{monthly median}$ ) for all these species. Figure 7-6 shows the correlation scatter plots between  $\Delta C_3H_8$  and  $\Delta CH_4$ ,  $\Delta CO$ ,  $\Delta C_2H_2$ , and  $\Delta C_2H_6$ . High correlation coefficients (R) are found between  $\Delta C_3H_8$  and  $\Delta C_2H_6$  (R=0.84), and between  $\Delta C_3H_8$  and  $\Delta C_2H_2$  (R=0.79). It indicates that the C<sub>2</sub>H<sub>2</sub>, C<sub>2</sub>H<sub>6</sub> and C<sub>3</sub>H<sub>8</sub> (NMHCs) are co-emitted in this region. The slope of  $\Delta C_2H_6$  and  $\Delta C_3H_8$  is  $6.03 \pm 0.03$ , which suggests a corresponding mixing ratio of C<sub>2</sub>H<sub>6</sub> and C<sub>3</sub>H<sub>8</sub> mole fractions during the production in North China. CO, as a pollutant tracer, also has a good correlation with C<sub>3</sub>H<sub>8</sub> (R=0.72). According to the MEIC inventory, both CO and NMHC are emitted from the energy production, industry, residential and transport sectors.

The FTIR measurements show that the correlation between  $\Delta C_3H_8$  and  $\Delta CH_4$  is relatively weak (R=0.45). Note that the variation of the CH<sub>4</sub> column is also affected by the stratospheric partial column (Sepúlveda et al., 2014). The DOF of the FTIR CH<sub>4</sub> retrieval is about 2.5 allowing us to derive the tropospheric and stratospheric CH<sub>4</sub> partial columns separately (Zhou et al., 2018). However, even after eliminating the interference from the stratosphere, the tropospheric CH<sub>4</sub> partial column still **have** **has** a weak correlation with C<sub>3</sub>H<sub>8</sub> (R=0.43). It is probably due to **the fact** that the CH<sub>4</sub> major emissions in North China are from rice cultivation, waste, and animals instead of the oil and gas production (Ji et al., 2020), and the CH<sub>4</sub> measurements include the emissions from much farther away as compared to the C<sub>3</sub>H<sub>8</sub> measurements because of its long lifetime (Callewaert et al., 2023).

To further investigate the ratio of  $\Delta C_2H_6$  to  $\Delta C_3H_8$ , the time series of their ratios, together with the monthly correlation coefficients between both time series between June 2018 and June 2022 are illustrated in Figure 8-7. The ratio of each month is derived from the linear fitting using all co-located  $\Delta C_2H_6$  and  $\Delta C_3H_8$  hourly measurements in that month. A relatively low correlation between these two species is found in summer as compared to other three seasons. The mean and std of the ratios are  $5.4 \pm 2.1$  for the whole period. The ratio is lowest in summer and highest in winter, with seasonal means of 6.6, 3.8, 5.4, and 8.3 in spring, summer, autumn, and winter, respectively.

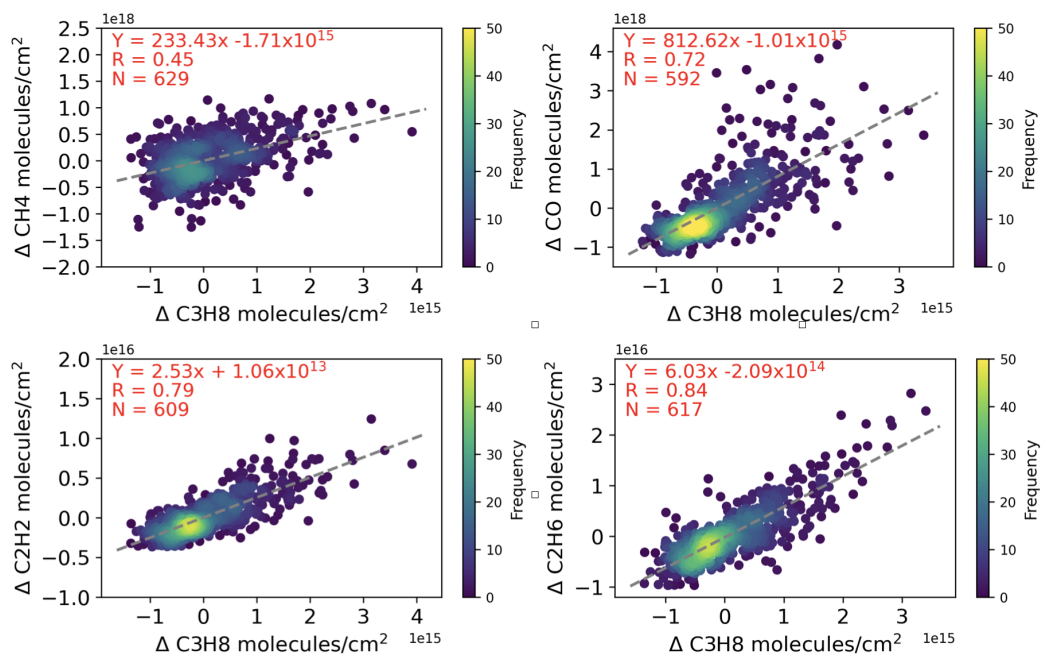


**Figure 6.** The correlation plots between co-located  $\Delta C_3H_8$  and  $\Delta CH_4$ ,  $\Delta CO$ ,  $\Delta C_2H_2$  and  $\Delta C_2H_6$  hourly means at Xianghe between June 2018 and July 2022. The grey dashed line is the linear fit,  $N$  is the number of the FTIR measurements,  $R$  is the Pearson correlation coefficient.

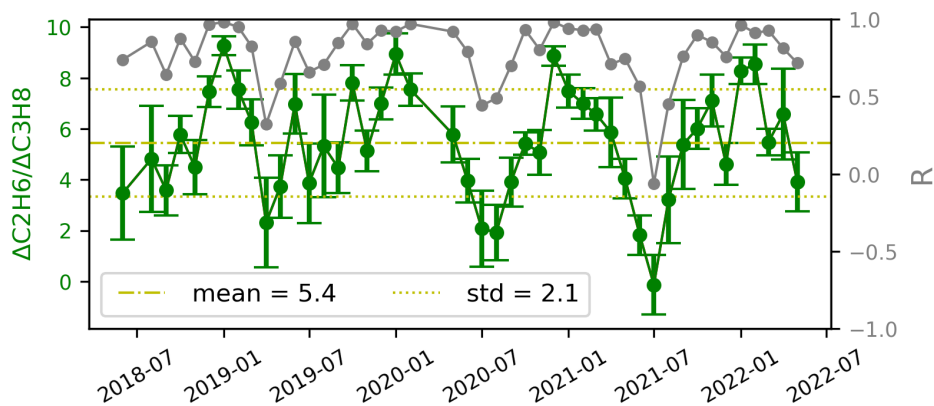


**Figure 7.** The time series of the ratio of  $\Delta C_2H_6$  to  $\Delta C_3H_8$  monthly means and stds (green, on the left-hand vertical axis scale), together with their monthly correlation coefficients (grey, on the right-hand vertical axis scale) between June 2018 and June 2022.

### 3.3 FTIR measurements at Xianghe against MkIV measurements

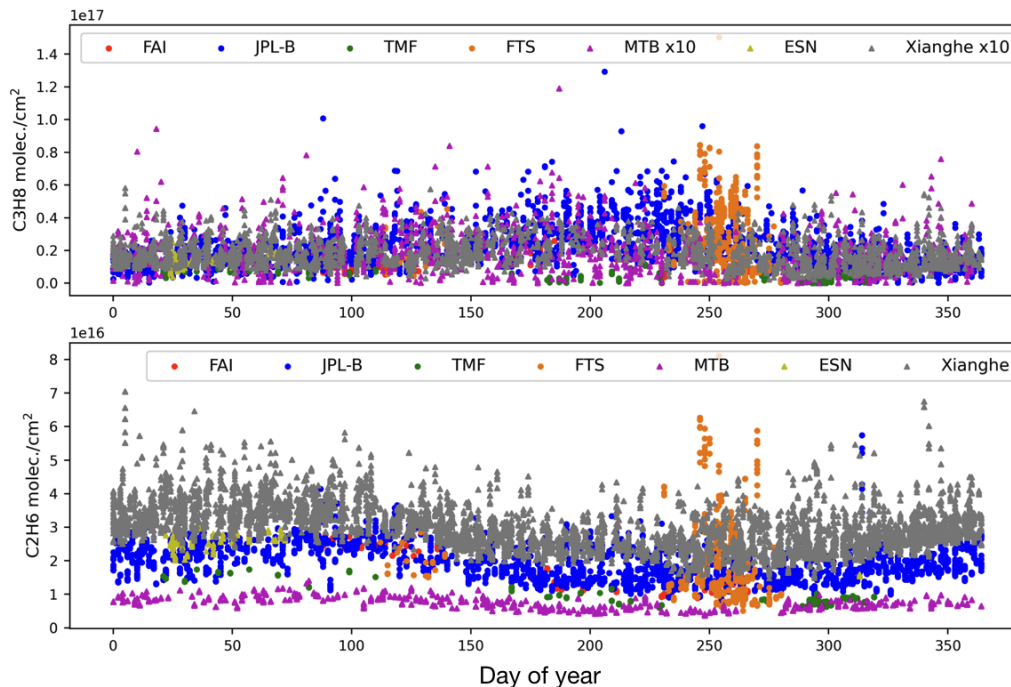
Here, the  $C_3H_8$  and  $C_2H_6$  columns derived from the FTIR measurements at Xianghe are compared to the ground-based MKIV  $C_3H_8$  retrievals at 6 sites in Sweden and the USA (Figure 9). ~~Note that 8). MKIV data uses the GFIT inverse retrieval code to derive the  $C_3H_8$  columns from the MKIV observed spectra between 2964.5 and 2970  $cm^{-1}$  with a spectral resolution of 0.5  $cm^{-1}$ . The mean uncertainties of the MKIV retrieved  $C_3H_8$  and  $C_2H_6$  column are estimated to be around  $8 \times 10^{15} molec./cm^2$  and  $7 \times 10^{14} molec./cm^2$ , respectively (Toon et al., 2021). Note that, the  $C_3H_8$  and  $C_2H_6$  retrievals from the MkIV spectrometers at 12 sites have been discussed in Toon et al. (2021), and we only select 6 sites as the measurements are very limited at other 6 sites. The locations and measurement time coverages of sites used in this study are listed in Table 4.~~

Figure 9.8 shows that the  $C_2H_6$  column is the largest at Xianghe, apart from several extremely high values at JPL-B and FTS. The seasonal variations of  $C_2H_6$  columns are similar at these sites, especially for JPL-B, MTB and Xianghe, with a high value in northern spring and a low value in northern autumn. Note that, it is hard to derive the seasonal variation of  $C_2H_6$  columns at ESN, FAI, TMF and FTS, because measurements were carried out in several months. The mean and std of  $C_2H_6$  columns at JPL-B are  $1.96 \pm 0.52 \times 10^{16} molec./cm^2$ , which is about 25% less than that at Xianghe ((Xianghe-JPL)/Xianghe  $\times 100\%$ ). Keep in mind that the  $C_3H_8$  columns at MTB and Xianghe have been multiplied by 10 in Figure 9.8. The  $C_3H_8$  column at Xianghe is quite low as compared to other sites, which is only larger than that at MTB (mountain site), but much less than those at the mid-latitude sites. The mean and std of  $C_3H_8$  columns at JPL-B are  $2.14 \pm 1.33 \times 10^{16} molec./cm^2$ , which is about 12 times larger than that at Xianghe. The seasonal variations of  $C_3H_8$  columns are similar at JPL-B and Xianghe too, with a high value in northern summer and a low value in northern winter. The good correlations ( $R > 0.6$ ) between  $C_3H_8$  and  $C_2H_6$  columns at JPL-B and FTS have been demonstrated in Toon et al. (2021), which is similar to what we observe at Xianghe. However, the ratio of  $\Delta C_2H_6$  to  $\Delta C_3H_8$  at JPL-B and FTS are  $0.16 \pm 0.10$  and  $0.78 \pm 0.10$ , respectively, which are much less than the ratio observed at Xianghe of  $6.03 \pm 0.03$ . It indicates that the emission of  $C_3H_8$  is much larger in the Los Angeles basin, California than that in North China.

## 4 Conclusions

The Xianghe FTIR 125HR system measures the solar absorption spectra following the NDACC-IRWG guidance. For the first time, the FTIR MIR spectra at Xianghe are used for the  $C_3H_8$  column retrieval, using the well-established SFIT4 code, between June 2018 and July 2022. In this study, the retrieval strategy, retrieval uncertainty, and retrieval information are presented and discussed. Due to the wide and weak absorption of  $C_3H_8$ , we only derive the  $C_3H_8$  column instead of its vertical profile. The systematic and random uncertainties of the  $C_3H_8$  retrieved column are estimated to be ~~18.2~~18.4% and 18.1%, respectively. In the  $C_3H_8$  retrieval window,  $CH_4$  and  $H_2O$  absorption lines are not perfectly fitted, indicating there is still room left to improving the line lists of these two species.

The mean and std of the  $C_3H_8$  column derived from the FTIR measurements at Xianghe are  $1.80 \pm 0.81 \times 10^{15} molec./cm^2$ . A month-to-month variation is observed with a high value in July and a low value in October. The difference between the median values in July (maximum) and October (minimum) is  $1.2 \times 10^{15} molec./cm^2$ . ~~The FTIR  $C_3H_8$  column retrievals are~~



**Figure 8.** The  $C_3H_8$  (upper panel) and  $C_2H_6$  (lower panel) columns observed by ground-based Bruker IFS 125HR at Xianghe and MkIV spectrometer at 6 sites. Note that the  $C_3H_8$  columns observed at MTB and Xianghe are multiplied by 10 to have a better view.

**Table 4.** The locations, and data time coverages of the MkIV measurements at 6 sites, together with their mean  $C_3H_8$  and  $C_2H_6$  columns. The bottom row is the Xianghe FTIR measurements in this study.

Site	Country	Latitude	Longitude	Altitude (km)	Time coverage	$C_3H_8$ (molec./cm <sup>2</sup> )	$C_2H_6$ (molec./cm <sup>2</sup> )
Esrang(ESN)	Sweden	67.89°N	21.08°E	0.271	Nov 1999 - Mar 2020	$1.4 \times 10^{16}$	$2.6 \times 10^{16}$
Fairbanks(FAI)	USA	64.83°N	147.61°W	0.182	Mar-Sep 1997	$1.4 \times 10^{16}$	$1.8 \times 10^{16}$
Mt. Barcroft(MTB)	USA	37.58°N	118.23°W	3.801	Oct 1998 - Aug 2002	$1.4 \times 10^{15}$	$7.3 \times 10^{15}$
Ft. Sumner(FTS)	USA	34.48°N	104.22°W	1.260	Oct 1989 - Sep 2021	$2.6 \times 10^{16}$	$1.9 \times 10^{16}$
TMF, Wrightwood (TMF)	USA	34.38°N	117.68°W	2.257	Jul-Sep 1988; Nov 1996 Jan-Aug 1998; Oct 2009	$2.7 \times 10^{15}$	$8.3 \times 10^{15}$
JPL B183(JPL-B)	USA	34.20°N	118.17°W	0.345	Jun 1985 - Jan 2022	$2.1 \times 10^{16}$	$2.0 \times 10^{16}$
Xianghe	China	39.75°N	116.96°E	0.036	Jun 2018 - Jul 2022	$1.8 \times 10^{15}$	$3.0 \times 10^{16}$

compared to two well-known models (CAM5 and WACCM). It is found that the mean  $C_3H_8$  columns from the two models are 68% larger than the FTIR measurements at Xianghe, which is beyond the systematic uncertainty of our FTIR retrieval.

Moreover, the seasonal variations of the C<sub>3</sub>H<sub>8</sub> column derived from CAMS and WACCM models also deviates from that derived from the FTIR measurements. Further investigations are needed to better understand the mismatch between the model simulations and FTIR measurements, and to improve the C<sub>3</sub>H<sub>8</sub> model simulations at Xianghe.

As C<sub>3</sub>H<sub>8</sub> are co-emitted with CH<sub>4</sub>, CO, C<sub>2</sub>H<sub>2</sub>, and C<sub>2</sub>H<sub>6</sub> during oil and gas production, we calculate the correlation between  $\Delta$ C<sub>3</sub>H<sub>8</sub> and these species at Xianghe. Good correlations are found between C<sub>3</sub>H<sub>8</sub> and C<sub>2</sub>H<sub>6</sub>, between C<sub>3</sub>H<sub>8</sub> and C<sub>2</sub>H<sub>2</sub>, as well as between C<sub>3</sub>H<sub>8</sub> and CO. However, the correlation between C<sub>3</sub>H<sub>8</sub> and CH<sub>4</sub> is relatively weak, which is probably due to CH<sub>4</sub> emission in North China being dominated by rice, cultivation, and waste, instead of oil and gas production and fossil fuels combustion. By comparing the C<sub>3</sub>H<sub>8</sub> and C<sub>2</sub>H<sub>6</sub> columns at Xianghe with 6 other sites around the world, provided by the ground-based MkIV spectrometers, we find that the C<sub>2</sub>H<sub>6</sub> column at Xianghe is the largest. However, the C<sub>3</sub>H<sub>8</sub> column at Xianghe is only larger than those observed at the mountain sites and polar sites, and it is much less than the C<sub>3</sub>H<sub>8</sub> columns observed at mid-latitude sites in the USA. Currently, the reported uncertainty of MKIV C<sub>3</sub>H<sub>8</sub> measurements is relatively large of about  $8 \times 10^{15}$  molec./cm<sup>2</sup>, which is much larger than the mean FTIR C<sub>3</sub>H<sub>8</sub> measurements at Xianghe. Further investigation is needed to understand the large difference between FTIR and MKIV C<sub>3</sub>H<sub>8</sub> measurements.

In summary, we successfully retrieve C<sub>3</sub>H<sub>8</sub> columns from the FTIR MIR spectra at Xianghe, which provides us with a new dataset to understand the variation of C<sub>3</sub>H<sub>8</sub> in North China. The retrieval strategy of C<sub>3</sub>H<sub>8</sub> in this study should work at other Bruker 125HR FTIR sites as well, especially for those close to a city or oil and gas field, e.g., Paris, Toronto, and Boulder. Nevertheless, efforts are still needed within the NDACC-IWRG community to generate a global harmonized FTIR C<sub>3</sub>H<sub>8</sub> column dataset.

*Data availability.* The ground-based MkIV C<sub>3</sub>H<sub>8</sub> and C<sub>2</sub>H<sub>6</sub> retrievals are publicly available via <https://mark4sun.jpl.nasa.gov/ground.html> (last access date: 27 September 2022). The FTIR C<sub>3</sub>H<sub>8</sub> retrievals at Xianghe are available upon request. The WACCM model data are publicly available via <https://www.acom.ucar.edu/waccm/download.shtml> (last access date: 27 March 2024).

*Competing interests.* The authors declare that they have no conflict of interest.

*Acknowledgements.* The author would like to thank the NDACC community for supporting the SFIT4 retrieval algorithm. We would acknowledge all Xianghe site staffs, Nicolas Kumps (BIRA-IASB) for the FTIR instrument maintenance. This study is supported by the National key research and development program (2023YFC3705202).

*Author contributions.* PW and MZ design the study and wrote the manuscript. MZ, BL, BD, MDM investigated the SFIT4 retrieval strategy. WN, CH and QC operate the FTIR measurements at Xianghe. GT provides the MKIV measurements. All authors have read and commented the manuscript.

## References

- Blumenstock, T., Hase, F., Keens, A., Czurlok, D., Colebatch, O., Garcia, O., Griffith, D. W. T., Grutter, M., Hannigan, J. W., Heikkinen, P., Jeseck, P., Jones, N., Kivi, R., Lutsch, E., Makarova, M., Imhasin, H. K., Mellqvist, J., Morino, I., Nagahama, T., Notholt, J., Ortega, I., Palm, M., Raffalski, U., Rettinger, M., Robinson, J., Schneider, M., Servais, C., Smale, D., Stremme, W., Strong, K., Sussmann, R., Té, Y., and Velazco, V. A.: Characterization and potential for reducing optical resonances in Fourier transform infrared spectrometers of the Network for the Detection of Atmospheric Composition Change (NDACC), *Atmos. Meas. Tech.*, 14, 1239–1252, <https://doi.org/10.5194/amt-14-1239-2021>, 2021.
- Bourtsoukidis, E., Ernle, L., Crowley, J. N., Lelieveld, J., Paris, J.-D., Pozzer, A., Walter, D., and Williams, J.: Non-methane hydrocarbon ( $C_2$ – $C_8$ ) sources and sinks around the Arabian Peninsula, *Atmos. Chem. Phys.*, 19, 7209–7232, <https://doi.org/10.5194/acp-19-7209-2019>, 2019.
- Callewaert, S., Zhou, M., Langerock, B., Wang, P., Wang, T., Mahieu, E., and De Mazière, M.: A WRF-Chem study on the variability of  $CO_2$ ,  $CH_4$  and CO concentrations at Xianghe, China supported by ground-based observations and TROPOMI, *EGUsphere*, 2023, 1–37, <https://doi.org/10.5194/egusphere-2023-2103>, 2023.
- Crippa, M., Solazzo, E., Huang, G., Guizzardi, D., Koffi, E., Muntean, M., Schieberle, C., Friedrich, R., and Janssens-Maenhout, G.: High resolution temporal profiles in the Emissions Database for Global Atmospheric Research, *Sci. Data*, 7, 121, <https://doi.org/10.1038/s41597-020-0462-2>, 2020.
- De Mazière, M., Thompson, A. M., Kurylo, M. J., Wild, J. D., Bernhard, G., Blumenstock, T., Braathen, G. O., Hannigan, J. W., Lambert, J.-C., Leblanc, T., McGee, T. J., Nedoluha, G., Petropavlovskikh, I., Seckmeyer, G., Simon, P. C., Steinbrecht, W., and Strahan, S. E.: The Network for the Detection of Atmospheric Composition Change (NDACC): history, status and perspectives, *Atmos. Chem. Phys.*, 18, 4935–4964, <https://doi.org/10.5194/acp-18-4935-2018>, 2018.
- Donahue, N. M. and Prinn, R. G.: Nonmethane hydrocarbon chemistry in the remote marine boundary layer, *Journal of Geophysical Research: Atmospheres*, 95, 18 387–18 411, <https://doi.org/https://doi.org/10.1029/JD095iD11p18387>, 1990.
- Franco, B., Mahieu, E., Emmons, L. K., Tzompa-Sosa, Z. A., Fischer, E. V., Sudo, K., Bovy, B., Conway, S., Griffin, D., Hannigan, J. W., Strong, K., and Walker, K. A.: Evaluating ethane and methane emissions associated with the development of oil and natural gas extraction in North America, *Environ. Res. Lett.*, 11, 044 010, <https://doi.org/10.1088/1748-9326/11/4/044010>, 2016.
- Gottelman, A., Mills, M. J., Kinnison, D. E., Garcia, R. R., Smith, A. K., Marsh, D. R., Tilmes, S., Vitt, F., Bardeen, C. G., McInerny, J., Liu, H.-L., Solomon, S. C., Polvani, L. M., Emmons, L. K., Lamarque, J.-F., Richter, J. H., Glanville, A. S., Bacmeister, J. T., Phillips, A. S., Neale, R. B., Simpson, I. R., DuVivier, A. K., Hodzic, A., and Randel, W. J.: The Whole Atmosphere Community Climate Model Version 6 (WACCM6), *J. Geophys. Res. Atmos.*, 124, 12 380–12 403, <https://doi.org/https://doi.org/10.1029/2019JD030943>, 2019.
- Gordon, I., Rothman, L., Hargreaves, R., Hashemi, R., Karlovets, E., Skinner, F., Conway, E., Hill, C., Kochanov, R., Tan, Y., Weislo, P., Finenko, A., Nelson, K., Bernath, P., Birk, M., Boudon, V., Campargue, A., Chance, K., Coustenis, A., Drouin, B., Flaud, J., Gamache, R., Hodges, J., Jacquemart, D., Mlawer, E., Nikitin, A., Perevalov, V., Rotger, M., Tennyson, J., Toon, G., Tran, H., Tyuterev, V., Adkins, E., Baker, A., Barbe, A., Canè, E., Császár, A., Dudaryonok, A., Egorov, O., Fleisher, A., Fleurbaey, H., Foltynowicz, A., Furtenbacher, T., Harrison, J., Hartmann, J., Horneman, V., Huang, X., Karman, T., Karns, J., Kass, S., Kleiner, I., Kofman, V., Kwabia-Tchana, F., Lavrentieva, N., Lee, T., Long, D., Lukashovskaya, A., Lyulin, O., Makhnev, V., Matt, W., Massie, S., Melosso, M., Mikhailenko, S., Mondelain, D., Müller, H., Naumenko, O., Perrin, A., Polyansky, O., Raddaoui, E., Raston, P., Reed, Z., Rey, M., Richard, C., Tóbiás, R., Sadiq, I., Schwenke, D., Starikova, E., Sung, K., Tamassia, F., Tashkun, S., Vander Auwera, J., Vasilenko, I., Viganin, A., Villanueva,

- G., Vispoel, B., Wagner, G., Yachmenev, A., and Yurchenko, S.: The HITRAN2020 molecular spectroscopic database, *J Quant Spectrosc Radiat Transf.*, 277, 107 949, <https://doi.org/https://doi.org/10.1016/j.jqsrt.2021.107949>, 2022.
- Harrison, J. J., Allen, N. D., and Bernath, P. F.: Infrared absorption cross sections for ethane (C<sub>2</sub>H<sub>6</sub>) in the 3  $\mu$ m region, *J. Quant. Spectrosc. Radiat. Transf.*, 111, 357–363, <https://doi.org/10.1016/J.QSRT.2009.09.010>, 2010.
- 5 Hase, F., Hannigan, J., Coffey, M., Goldman, A., Höpfner, M., Jones, N., Rinsland, C., and Wood, S.: Intercomparison of retrieval codes used for the analysis of high-resolution, ground-based FTIR measurements, *J. Quant. Spectrosc. Radiat. Transf.*, 87, 25 – 52, <https://doi.org/10.1016/j.jqsrt.2003.12.008>, 2004.
- Inness, A., Ades, M., Agustí-Panareda, A., Barré, J., Benedictow, A., Blechschmidt, A.-M., Dominguez, J. J., Engelen, R., Eskes, H., Flemming, J., Huijnen, V., Jones, L., Kipling, Z., Massart, S., Parrington, M., Peuch, V.-H., Razinger, M., Remy, S., Schulz, M., and Suttie,
- 10 M.: The CAMS reanalysis of atmospheric composition, *Atmos. Chem. Phys.*, 19, 3515–3556, <https://doi.org/10.5194/acp-19-3515-2019>, 2019.
- IPCC: Climate change 2013: The physical science basis. Contribution of Working Group I to the Fifth Assessment Report of the Intergovernmental Panel on Climate Change, 2013.
- Jacob, D. J.: Introduction to Atmospheric Chemistry, Princeton University Press, <http://www.jstor.org/stable/j.ctt7t8hg>, 1999.
- 15 Ji, D., Zhou, M., Wang, P., Yang, Y., Wang, T., Sun, X., Hermans, C., Yao, B., and Wang, G.: Deriving Temporal and Vertical Distributions of Methane in Xianghe Using Ground-based Fourier Transform Infrared and Gas-analyzer Measurements, *Adv. Atmos. Sci.*, 37, 597–607, <https://doi.org/10.1007/s00376-020-9233-4>, 2020.
- Kort, E. A., Smith, M. L., Murray, L. T., Gvakharia, A., Brandt, A. R., Peischl, J., Ryerson, T. B., Sweeney, C., and Travis, K.: Fugitive emissions from the Bakken shale illustrate role of shale production in global ethane shift, *Geophys. Res. Lett.*, 43, 4617–4623,
- 20 <https://doi.org/https://doi.org/10.1002/2016GL068703>, 2016.
- Lelieveld, J., Evans, J. S., Fnais, M., Giannadaki, D., and Pozzer, A.: The contribution of outdoor air pollution sources to premature mortality on a global scale, *Nature*, 525, 367–371, <https://doi.org/10.1038/nature15371>, 2015.
- Li, M., Liu, H., Geng, G., Hong, C., Liu, F., Song, Y., Tong, D., Zheng, B., Cui, H., Man, H., Zhang, Q., and He, K.: Anthropogenic emission inventories in China: a review, *Natl. Sci. Rev.*, 4, 834–866, <https://doi.org/10.1093/nsr/nwx150>, 2017.
- 25 Li, M., Pozzer, A., Lelieveld, J., and Williams, J.: Northern hemispheric atmospheric ethane trends in the upper troposphere and lower stratosphere (2006–2016) with reference to methane and propane, *Earth Syst. Sci. Data*, 14, 4351–4364, <https://doi.org/10.5194/essd-14-4351-2022>, 2022.
- Loos, J., Birk, M., and Wagner, G.: Measurement of air-broadening line shape parameters and temperature dependence parameters of H<sub>2</sub>O lines in the spectral ranges 1850–2280 cm<sup>-1</sup> and 2390–4000 cm<sup>-1</sup>, *J. Quant. Spectrosc. Radiat. Transf.*, 203, 103–118,
- 30 <https://doi.org/10.1016/J.QSRT.2017.03.033>, 2017.
- Marsh, D. R., Mills, M. J., Kinnison, D. E., Lamarque, J.-F., Calvo, N., and Polvani, L. M.: Climate Change from 1850 to 2005 Simulated in CESM1(WACCM), *J. Clim.*, 26, 7372–7391, <https://doi.org/10.1175/JCLI-D-12-00558.1>, 2013.
- Ortega, I., Buchholz, R. R., Hall, E. G., Hurst, D. F., Jordan, A. F., and Hannigan, J. W.: Tropospheric water vapor profiles obtained with FTIR: comparison with balloon-borne frost point hygrometers and influence on trace gas retrievals, *Atmos. Meas. Tech.*, 12, 873–890,
- 35 <https://doi.org/10.5194/amt-12-873-2019>, 2019.
- Pougatchev, N. S., Connor, B. J., and Rinsland, C. P.: Infrared measurements of the ozone vertical distribution above Kitt Peak, *J. Geophys. Res.*, 100, 16 689, <https://doi.org/10.1029/95JD01296>, 1995.



- Rigby, M., Montzka, S. A., Prinn, R. G., White, J. W. C., Young, D., O'Doherty, S., Lunt, M. F., Ganesan, A. L., Manning, A. J., Simmonds, P. G., Salameh, P. K., Harth, C. M., Mühle, J., Weiss, R. F., Fraser, P. J., Steele, L. P., Krummel, P. B., McCulloch, A., and Park, S.: Role of atmospheric oxidation in recent methane growth, *Proc. Natl. Acad. Sci.*, 114, 5373–5377, <https://doi.org/10.1073/pnas.1616426114>, 2017.
- 5 Rodgers, C. D.: *Inverse Methods for Atmospheric Sounding – Theory and Practice*, Series on Atmospheric Oceanic and Planetary Physics, vol. 2, World Scientific Publishing Co. Pte. Ltd, Singapore, <https://doi.org/10.1142/9789812813718>, 2000.
- Saha, S., Moorthi, S., Wu, X., Wang, J., Nadiga, S., Tripp, P., Behringer, D., Hou, Y.-T., ya Chuang, H., Iredell, M., Ek, M., Meng, J., Yang, R., Mendez, M. P., van den Dool, H., Zhang, Q., Wang, W., Chen, M., and Becker, E.: The NCEP Climate Forecast System Version 2, *J. Clim.*, 27, 2185 – 2208, <https://doi.org/10.1175/JCLI-D-12-00823.1>, 2014.
- 10 Saunio, M., Stavert, A. R., Poulter, B., Bousquet, P., Canadell, J. G., Jackson, R. B., Raymond, P. A., Dlugokencky, E. J., Houweling, S., Patra, P. K., Ciais, P., Arora, V. K., Bastviken, D., Bergamaschi, P., Blake, D. R., Brailsford, G., Bruhwiler, L., Carlson, K. M., Carrol, M., Castaldi, S., Chandra, N., Crevoisier, C., Crill, P. M., Covey, K., Curry, C. L., Etiope, G., Frankenberg, C., Gedney, N., Hegglin, M. I., Höglund-Isaksson, L., Hugelius, G., Ishizawa, M., Ito, A., Janssens-Maenhout, G., Jensen, K. M., Joos, F., Kleinen, T., Krummel, P. B., Langenfelds, R. L., Laruelle, G. G., Liu, L., Machida, T., Maksyutov, S., McDonald, K. C., McNorton, J., Miller, P. A., Melton, J. R.,
- 15 Morino, I., Müller, J., Murguía-Flores, F., Naik, V., Niwa, Y., Noce, S., O'Doherty, S., Parker, R. J., Peng, C., Peng, S., Peters, G. P., Prigent, C., Prinn, R., Ramonet, M., Regnier, P., Riley, W. J., Rosentretter, J. A., Segers, A., Simpson, I. J., Shi, H., Smith, S. J., Steele, L. P., Thornton, B. F., Tian, H., Tohjima, Y., Tubiello, F. N., Tsuruta, A., Viovy, N., Voulgarakis, A., Weber, T. S., van Weele, M., van der Werf, G. R., Weiss, R. F., Worthy, D., Wunch, D., Yin, Y., Yoshida, Y., Zhang, W., Zhang, Z., Zhao, Y., Zheng, B., Zhu, Q., Zhu, Q., and Zhuang, Q.: The Global Methane Budget 2000–2017, *Earth Syst. Sci. Data*, 12, 1561–1623, <https://doi.org/10.5194/essd-12-1561-2020>,
- 20 2020.
- Sepúlveda, E., Schneider, M., Hase, F., Barthlott, S., Dubravica, D., García, O. E., Gomez-Pelaez, A., González, Y., Guerra, J. C., Gisi, M., Kohlhepp, R., Dohe, S., Blumenstock, T., Strong, K., Weaver, D., Palm, M., Sadeghi, A., Deutscher, N. M., Warneke, T., Notholt, J., Jones, N., Griffith, D. W. T., Smale, D., Brailsford, G. W., Robinson, J., Meinhardt, F., Steinbacher, M., Aalto, T., and Worthy, D.: Tropospheric CH<sub>4</sub> signals as observed by NDACC FTIR at globally distributed sites and comparison to GAW surface in situ measurements, *Atmos. Meas. Tech.*, 7, 2337–2360, <https://doi.org/10.5194/amt-7-2337-2014>, 2014.
- 25 Sha, M. K., Langerock, B., Blavier, J.-F. L., Blumenstock, T., Borsdorff, T., Buschmann, M., Dehn, A., De Mazière, M., Deutscher, N. M., Feist, D. G., García, O. E., Griffith, D. W. T., Grutter, M., Hannigan, J. W., Hase, F., Heikkinen, P., Hermans, C., Iraci, L. T., Jeseck, P., Jones, N., Kivi, R., Kumpp, N., Landgraf, J., Lorente, A., Mahieu, E., Makarova, M. V., Mellqvist, J., Metzger, J.-M., Morino, I., Nagahama, T., Notholt, J., Ohyama, H., Ortega, I., Palm, M., Petri, C., Pollard, D. F., Rettinger, M., Robinson, J., Roche, S., Roehl, C. M.,
- 30 Röhling, A. N., Rousogonous, C., Schneider, M., Shiomi, K., Smale, D., Stremme, W., Strong, K., Sussmann, R., Té, Y., Uchino, O., Velasco, V. A., Vrekoussis, M., Wang, P., Warneke, T., Wizenberg, T., Wunch, D., Yamanouchi, S., Yang, Y., and Zhou, M.: Validation of Methane and Carbon Monoxide from Sentinel-5 Precursor using TCCON and NDACC-IRWG stations, *Atmos. Meas. Tech.*, 14, 6249–6304, <https://doi.org/10.5194/amt-14-6249-2021>, 2021.
- Steck, T.: Methods for determining regularization for atmospheric retrieval problems, *Appl. Opt.*, 41, 1788–1797, <https://doi.org/10.1364/AO.41.001788>, 2002.
- 35 Sze, N. D.: Anthropogenic CO Emissions: Implications for the Atmospheric CO-OH-CH<sub>4</sub> Cycle, *Science*, 195, 673–675, <https://doi.org/10.1126/science.195.4279.673>, 1977.

- Tan, J.-H., Guo, S.-J., Ma, Y.-L., Yang, F.-M., He, K.-B., Yu, Y.-C., Wang, J.-W., Shi, Z.-B., and Chen, G.-C.: Non-methane Hydrocarbons and Their Ozone Formation Potentials in Foshan, China, *Aerosol Air Qual. Res.*, 12, 387–398, <https://doi.org/10.4209/aaqr.2011.08.0127>, 2012.
- Thompson, C. R., Wofsy, S. C., Prather, M. J., Newman, P. A., Hanisco, T. F., Ryerson, T. B., Fahey, D. W., Apel, E. C., Brock, C. A., Brune, W. H., Froyd, K., Katich, J. M., Nicely, J. M., Peischl, J., Ray, E., Veres, P. R., Wang, S., Allen, H. M., Asher, E., Bian, H., Blake, D., Bourgeois, I., Budney, J., Bui, T. P., Butler, A., Campuzano-Jost, P., Chang, C., Chin, M., Commane, R., Correa, G., Crouse, J. D., Daube, B., Dibb, J. E., DiGangi, J. P., Diskin, G. S., Dollner, M., Elkins, J. W., Fiore, A. M., Flynn, C. M., Guo, H., Hall, S. R., Hannun, R. A., Hills, A., Hintsa, E. J., Hodzic, A., Hornbrook, R. S., Huey, L. G., Jimenez, J. L., Keeling, R. F., Kim, M. J., Kupc, A., Lacey, F., Lait, L. R., Lamarque, J.-F., Liu, J., McKain, K., Meinardi, S., Miller, D. O., Montzka, S. A., Moore, F. L., Morgan, E. J., Murphy, D. M., Murray, L. T., Nault, B. A., Neuman, J. A., Nguyen, L., Gonzalez, Y., Rollins, A., Rosenlof, K., Sargent, M., Schill, G., Schwarz, J. P., Clair, J. M. S., Steenrod, S. D., Stephens, B. B., Strahan, S. E., Strode, S. A., Sweeney, C., Thames, A. B., Ullmann, K., Wagner, N., Weber, R., Weinzierl, B., Wennberg, P. O., Williamson, C. J., Wolfe, G. M., and Zeng, L.: The NASA Atmospheric Tomography (ATom) Mission: Imaging the Chemistry of the Global Atmosphere, *Bull. Am. Meteorol. Soc.*, 103, E761 – E790, <https://doi.org/10.1175/BAMS-D-20-0315.1>, 2022.
- Tikhonov, A. N.: Solution of Incorrectly Formulated Problems and the Regularisation Method, *Soviet. Math. Dokl.*, 4, 1035–1038, 1963.
- Toon, G. C., Blavier, J.-F. L., Sung, K., and Yu, K.: Spectrometric measurements of atmospheric propane (C<sub>3</sub>H<sub>8</sub>), *Atmos. Chem. Phys.*, 21, 10727–10743, <https://doi.org/10.5194/acp-21-10727-2021>, 2021.
- Vigouroux, C., Langerock, B., Bauer Aquino, C. A., Blumenstock, T., Cheng, Z., De Mazière, M., De Smedt, I., Grutter, M., Hannigan, J. W., Jones, N., Kivi, R., Loyola, D., Lutsch, E., Mahieu, E., Makarova, M., Metzger, J.-M., Morino, I., Murata, I., Nagahama, T., Notholt, J., Ortega, I., Palm, M., Pinardi, G., Röhlings, A., Smale, D., Stremme, W., Strong, K., Sussmann, R., Té, Y., van Roozendael, M., Wang, P., and Winkler, H.: TROPOMI–Sentinel-5 Precursor formaldehyde validation using an extensive network of ground-based Fourier-transform infrared stations, *Atmos. Meas. Tech.*, 13, 3751–3767, <https://doi.org/10.5194/amt-13-3751-2020>, 2020.
- von Clarmann, T.: Smoothing error pitfalls, *Atmos. Meas. Tech.*, 7, 3023–3034, <https://doi.org/10.5194/amt-7-3023-2014>, 2014.
- Wang, M., Shao, M., Chen, W., Lu, S., Liu, Y., Yuan, B., Zhang, Q., Zhang, Q., Chang, C.-C., Wang, B., Zeng, L., Hu, M., Yang, Y., and Li, Y.: Trends of non-methane hydrocarbons (NMHC) emissions in Beijing during 2002–2013, *Atmos. Chem. Phys.*, 15, 1489–1502, <https://doi.org/10.5194/acp-15-1489-2015>, 2015.
- Wofsy, S. C.: HIPER Pole-to-Pole Observations (HIPPO): fine-grained, global-scale measurements of climatically important atmospheric gases and aerosols, *Philosophical Transactions of the Royal Society A: Mathematical, Physical and Engineering Sciences*, 369, 2073–2086, <https://doi.org/10.1098/rsta.2010.0313>, 2011.
- Xiao, Y., Logan, J. A., Jacob, D. J., Hudman, R. C., Yantosca, R., and Blake, D. R.: Global budget of ethane and regional constraints on U.S. sources, *J Geophys Res Atmos.*, 113, <https://doi.org/https://doi.org/10.1029/2007JD009415>, 2008.
- Yang, Y., Zhou, M., Langerock, B., Sha, M. K., Hermans, C., Wang, T., Ji, D., Vigouroux, C., Kumps, N., Wang, G., De Mazière, M., and Wang, P.: New ground-based Fourier-transform near-infrared solar absorption measurements of XCO<sub>2</sub>, XCH<sub>4</sub> and XCO at Xianghe, China, *Earth Syst. Sci. Data*, 12, 1679–1696, <https://doi.org/10.5194/essd-12-1679-2020>, 2020.
- Zhou, M., Vigouroux, C., Langerock, B., Wang, P., Dutton, G., Hermans, C., Kumps, N., Metzger, J.-M., Toon, G., and De Mazière, M.: CFC-11, CFC-12 and HCFC-22 ground-based remote sensing FTIR measurements at Réunion Island and comparisons with MIPAS/ENVISAT data, *Atmos. Meas. Tech.*, 9, 5621–5636, <https://doi.org/10.5194/amt-9-5621-2016>, 2016.

- Zhou, M., Langerock, B., Vigouroux, C., Sha, M. K., Ramonet, M., Delmotte, M., Mahieu, E., Bader, W., Hermans, C., Kumps, N., Metzger, J.-M., Duflot, V., Wang, Z., Palm, M., and De Mazière, M.: Atmospheric CO and CH<sub>4</sub> time series and seasonal variations on Reunion Island from ground-based in-situ and FTIR (NDACC and TCCON) measurements, *Atmos. Chem. Phys.*, 18, 13 881–13 901, <https://doi.org/10.5194/acp-18-13881-2018>, 2018.
- 5 Zhou, M., Wang, P., Langerock, B., Vigouroux, C., Hermans, C., Kumps, N., Wang, T., Yang, Y., Ji, D., Ran, L., Zhang, J., Xuan, Y., Chen, H., Posny, F., Duflot, V., Metzger, J.-M., and De Mazière, M.: Ground-based Fourier transform infrared (FTIR) O<sub>3</sub> retrievals from the 3040 cm<sup>-1</sup> spectral range at Xianghe, China, *Atmos. Meas. Tech.*, 13, 5379–5394, <https://doi.org/10.5194/amt-13-5379-2020>, 2020.
- Zhou, M., Langerock, B., Vigouroux, C., Dils, B., Hermans, C., Kumps, N., Nan, W., Metzger, J.-M., Mahieu, E., Wang, T., Wang, P., and De Mazière, M.: Tropospheric and stratospheric NO retrieved from ground-based Fourier-transform infrared (FTIR) measurements, *Atmos. Meas. Tech.*, 14, 6233–6247, <https://doi.org/10.5194/amt-14-6233-2021>, 2021.
- 10 Zhou, M., Langerock, B., Wang, P., Vigouroux, C., Ni, Q., Hermans, C., Dils, B., Kumps, N., Nan, W., and De Mazière, M.: Understanding the variations and sources of CO, C<sub>2</sub>H<sub>2</sub>, C<sub>2</sub>H<sub>6</sub>, H<sub>2</sub>CO, and HCN columns based on 3 years of new ground-based Fourier transform infrared measurements at Xianghe, China, *Atmos. Meas. Tech.*, 16, 273–293, <https://doi.org/10.5194/amt-16-273-2023>, 2023.